Stockholm University

Master Thesis

Degree Project in
Geoscience 45 hp

Assessing the response of vegetation to the end-Triassic mass extinction: A case study using *Classopollis* pollen from Pinhay Bay, UK

Bjarne Däcker



Stockholm 2024

Department of Geological Sciences
Stockholm University
SE-106 91 Stockholm

Abstract

The end-Triassic mass extinction (ETME), which took place ~201 million years ago, was one of the 'Big Five' mass extinctions of the Phanerozoic. This event resulted in extinctions both in marine and terrestrial environments, including a turnover of plant communities. Here I will investigate vegetation responses to the ETME using the pollen fossil record from a coastal sedimentary rock section at Pinhay Bay, near to Lyme Regis, Devon, UK. Pollen provide an abundant source of information to assess how plants responded to such events. These particles can record vegetational responses to environmental stresses, including those associated with mass extinctions, with aberrancies (deviations from the normal), including morphological changes, such as pollen assembled in clumps of multiple grains (multiples), size changes and darkened grains. This study focuses on the pollen genus *Classopollis*, which was produced by the now extinct conifer family Cheirolepidiaceae. Here I tested for possible aberrancies and polyploidy within *Classopollis* across the ETME, by examining changes in pollen size, the proportion of multiples relative to single grains, and symmetry (the relative size difference of individual pollen grains within multiples). The ETME is marked by a lithological change from Triassic limestone to Jurassic shale, associated with an increase in seawater depth. The average size and symmetry of *Classopollis* are larger after the transgression. Deeper water at the time of deposition selected for larger pollen and symmetric multiples, as these grains were more likely to float longer distances due to their higher surface area to volume ratio. Multiplicity remained relatively constant throughout the tested interval except for three peaks that can be linked to known episodes of volcanism and subsequent warming. Low symmetry among samples from the Triassic limestone as well as some small dark pollen indicate cases of stunted growth among *Classopollis* pollen. It been hypothesised that the Cheirolepids may have reacted to the ETME by doubling its genome, known as polyploidy. This theory was based on previous observations of unusually large *Classopollis* pollen. However, in this study no aberrantly large *Classopollis* pollen were found. In conclusion, these findings indicate that the conifer family Cheirolepidiaceae responded to the environmental stresses of ETME by changes to *Classopollis* pollen multiplicity, size and symmetry, but unlike many other plant groups survived this, and several other extinctions, and thus displayed a remarkable resilience.

Table of Contents

PROJECT GOALS **5**

INTRODUCTION **6**

MASS EXTINCTIONS 6
THE 'BIG FIVE' MASS EXTINCTIONS 6
CAUSES AND EFFECTS OF MASS EXTINCTIONS 6
THE TRIASSIC WORLD 9
TRIASSIC CLIMATES 9
CARNIAN PLUVIAL EPISODE 10
TRIASSIC ANIMALS 10
TRIASSIC PLANTS 11
THE END-TRIASSIC MASS EXTINCTION – ETME 12
EFFECTS OF THE ETME ON VEGETATION 15
EFFECTS OF THE ETME ON POLLEN AND SPORES 17
POLYPLOIDY 19
SUMMARY 20

GEOLOGICAL SETTING **21**

MATERIAL AND METHODS **24**

RESULTS **27**

MULTIPLICITY 28
POLLEN GRAIN SIZE 30
POLLEN MULTIPLE SYMMETRY 32
DARK SMALL POLLEN 33

DISCUSSION **34**

MULTIPLICITY 34
POLLEN GRAIN SIZE 35
POLLEN MULTIPLE SYMMETRY AND DARK SMALL POLLEN 36
POTTER CANYON 37
POLYPLOIDY 39
CLASSOPOLLIS RESILIENCE 40

CONCLUSIONS **41**

FUTURE WORK **41**

ACKNOWLEDGEMENTS **42**

REFERENCES **42**

APPENDIX 1. MULTIPLICITY **48**

APPENDIX 2. SIZE HISTOGRAMS **49**

APPENDIX 3. MULTIPLES FOUND WHEN MEASURING SIZE **51**

Project Goals

The end-Triassic mass extinction represents one of the so-called 'Big Five' mass extinctions in the fossil record. This event, which took place ~201 million years ago, was likely caused by an episode of massive volcanism linked to the opening of the Atlantic Ocean. One of the best fossil records to assess how vegetation responded to this extreme event is pollen and *Classopollis* pollen from the now extinct conifer family Cheirolepidiaceae are plentiful in the fossil material. Pollen react to environmental stresses by aberrancies (deviations from the normal) such as pollen multiples, small and darkened pollen grains or oversize pollen grains.

Plants with whole genome duplications are rare but can have higher adaptability and may have helped the angiosperms (flowering plants) to survive the end-Cretaceous mass extinction (Fawcett et al. 2009). Genome evolution is much slower in confers but a previous study had found evidence of whole genome doubling in *Classopollis* pollen in samples from Potter Canyon, Arizona (Leitch and Leitch 2012, Kürschner et al. 2013). Their hypothesis was that this enabled the Cheirolepids to endure the end-Triassic mass extinction.

The Swedish Museum of Natural History has samples collected from Pinhay Bay, UK, which are from the Triassic-Jurassic transition period, and which contain *Classopollis* pollen.

Research questions

1. Did any aberrancies occur among the *Classopollis* pollen from the Pinhay Bay site, UK, during the Triassic-Jurassic transition period?
2. Is there any indication of whole genome doubling among the *Classopollis* pollen from the Pinhay Bay site, UK, during this period?

These results will be compared with those of the previous project (Kürschner et al. 2013, Figure 1) to test their hypothesis and to draw conclusions whether this was a general trend or only a local occurrence. The project will make use of a microscope as well as photography and measurement software available at the Swedish Museum of Natural History.

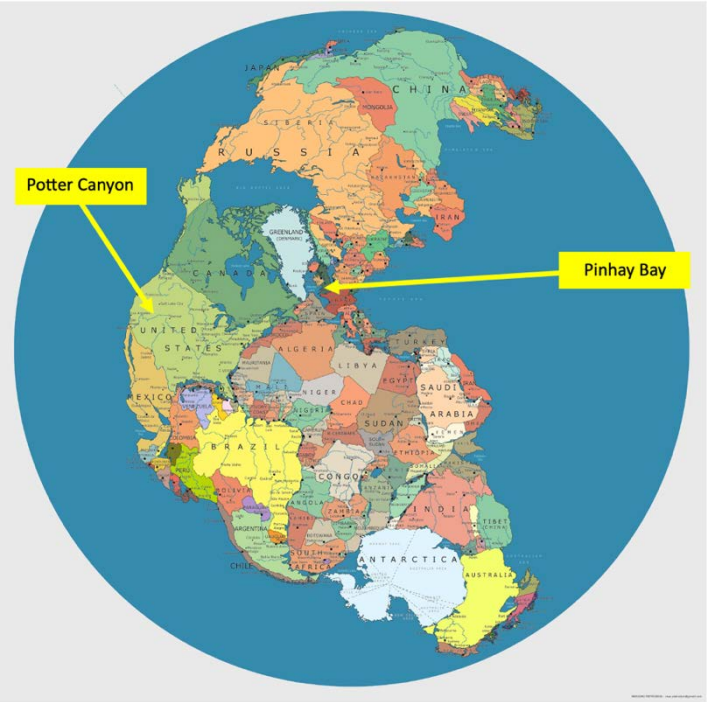


Figure 1.
Map of Pangea during the Triassic Period, 251.9 Mya to 201.4 Mya, with modern-day borders outlined (Routley, M. 2020).

Introduction

Mass extinctions

The end-Triassic mass extinction is one of a series of dramatic extinction events that have been identified in the fossil record. A mass extinction is a significant increase in the amount of extinctions during a short interval of geologic time, which results in a temporary reduction in diversity (Sepkoski 1986). Mass extinctions are significant events in the geologic history and many biostratigraphic boundaries are defined by mass extinctions (Ernst and Youbi 2017).

The 'Big Five' mass extinctions

There are five extinction events during the Cenozoic which are prominent in geologic history by having caused a loss of at least 75% of species and are defined as the 'Big Five' mass extinctions (Barnosky et al. 2011). Those five events are the end-Ordovician with 85% of species lost, the late-Devonian with 75% of species lost, the end-Permian with 95% of species lost, the end-Triassic with 80% of species lost and finally the end-Cretaceous with 75% of species lost (Ernst and Youbi 2017, Figure 2).

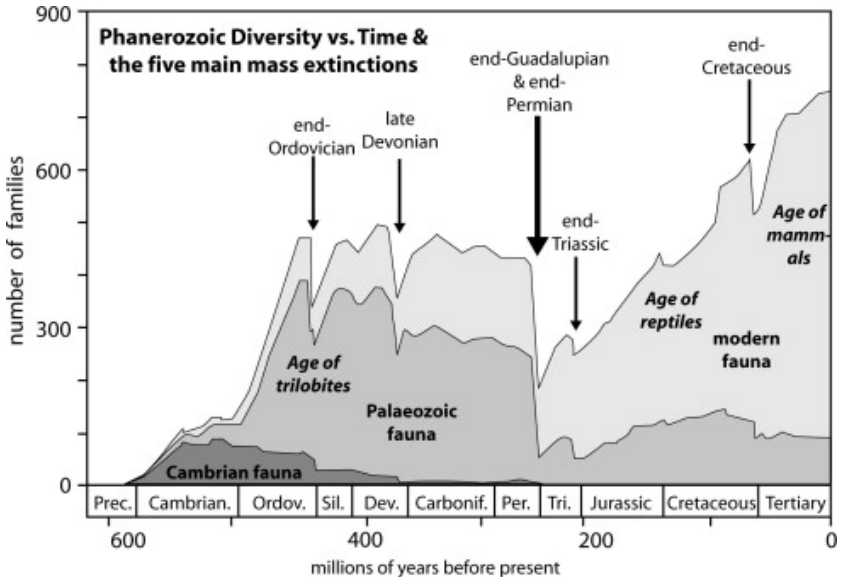


Figure 2. Phanerozoic diversity showing the three major faunas and the 'Big Five' mass extinctions (Metcalfe and Isozaki 2009).

Causes and effects of mass extinctions

A mass extinction starts by some initiating event which leads to a deterioration of the environment. That in turn undermines the living conditions for plants and animals which begin to die out. The initiating events can be bolide impacts from far outside the Earth, they can be related to plate tectonics, or they can be mantle plumes that rise from deep inside the Earth, push through the lithosphere and erupt as Large Igneous Provinces, LIPs (Bond and Grasby 2017). Remains of LIPs are found in many places on the Earth in the form of basaltic rocks, and it has been possible to link many of them to extinctions by matching extinction fossils with dates from high precision U-Pb measurements of the rocks (Ernst and Youbi

2017). Four of the 'Big Five' mass extinctions are linked to LIPs, such as the end-Permian mass extinction, which is called the "great dying" and is linked to the Siberian traps LIP, and the end-Triassic mass extinction which is associated with the Central Atlantic Magmatic Province (CAMP), one of the largest LIPs in Earth's history (Wignall 2001a). A mass extinction that is not linked to a LIP is the end-Ordovician mass extinction, which was in two pulses, first when Gondwana moved over the South pole and became glaciated, and second when the glaciation ended which led to rising sea-levels and transgressions (Bond and Grasby 2017). Circumstances play a part, a bolide that strikes in the ocean will cause a tsunami that creates chaos all around the Earth, on the other hand two large oceanic LIP's during the Cretaceous did not lead to any extinctions (Bond and Grasby 2017).

When a LIP is emplaced, large volumes of magma erupt and spread over the sea floor or land surface as flood basalt forming the province. At the same time, gases that accompany the magma spread through the atmosphere and affect the environment on a global scale (Bond and Grasby 2017). The most important volcanic gas is the greenhouse gas CO_2. During the end-Permian mass extinction the volume of CO_2 was so large that global temperatures rose by 10°C above previous levels (Bond and Grasby 2017). Another greenhouse gas that also causes acid rain is SO_2 which, however, after some time instead forms aerosols that absorb incoming sunlight possibly leading to photosynthetic shutdown and volcanic winters (Wignall 2001a).

Other volcanic gases are chlorine and fluorine which deplete the ozone layer with increased mutagenic UV-B radiation as result (Bond and Grasby 2017). Gases that also contribute to acid rain but do not remain long in the atmosphere are H_2SO_4, HCl and HF (Wignall 2001a, Figure 3). LIPs also spread toxic metals such as Hg, Os, Fe, Mo, Pb, Mn and As. Mercury, Hg, which is lethal to life can be distributed widely since metallic mercury is volatile (Thibodeau et al. 2016, Ernst and Youbi 2017). Such poisonous gases and other metals released during LIP emplacement are considered a significant factor and potential 'kill mechanism' in several major mass extinctions.

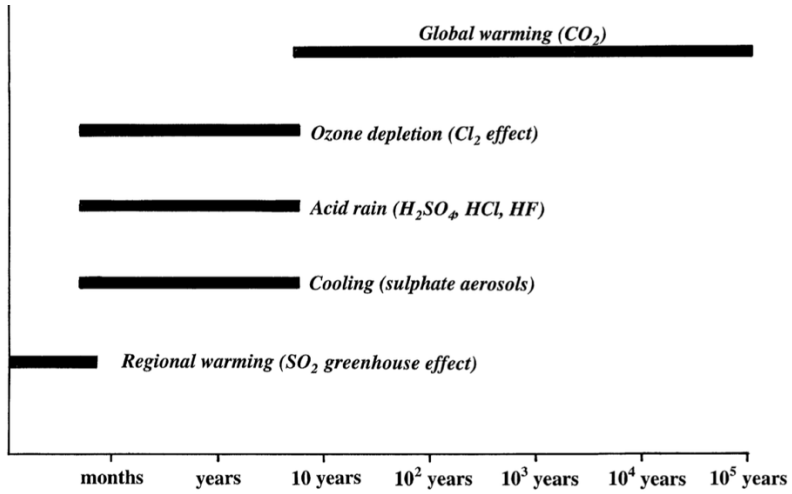


Figure 3. Effects of volcanic gases and how long they remain in the atmosphere (Wignall 2001a).

Acid rain from CO_2 and other gases escalates weathering on land causing erosion. When the vegetation weakens or dies, erosion increases even further resulting in sediment flux to the oceans (Bond and Grasby 2017, Benton 2016). Acidic oceans lead to calcified marine biota dying off (Ernst and Youbi 2017). Warming and CO_2 cause marine anoxia, extinction, and the deposition of black shale (Bond and Grasby 2017, Benton 2016).

When a mantle plume pushes upwards it causes earthquakes on a large scale as well as transgressions (Simms 2007, Ernst and Youbi 2017). It can encounter and burn organic-rich sediments and coal seams which produce even more CO_2 (Bond and Grasby 2017). Increased wildfires also contribute CO_2 plus polluting smoke (Ernst and Youbi 2017). Methane, CH_4, is stored in the oceans as gas hydrates which can start melting because of the warming thus releasing CH_4 which causes even more warming in a feed-back loop. Since CH_4 is twenty times more powerful as a greenhouse gas than CO_2 this can explain the rapid global warming during the end-Permian and the end-Triassic mass extinctions (Bond and Grasby 2017).

The deterioration of the environment consists of many killing processes such as warming, arctic winter, volcanic darkness, poisoning, ozone depletion, UV radiation, wildfires, erosion, acid rain, transgressions and anoxia, often together. Some of those processes trigger other processes leading to a cascade of destruction (Bond and Grasby 2017, Ernst and Youbi 2017, Figure 4).

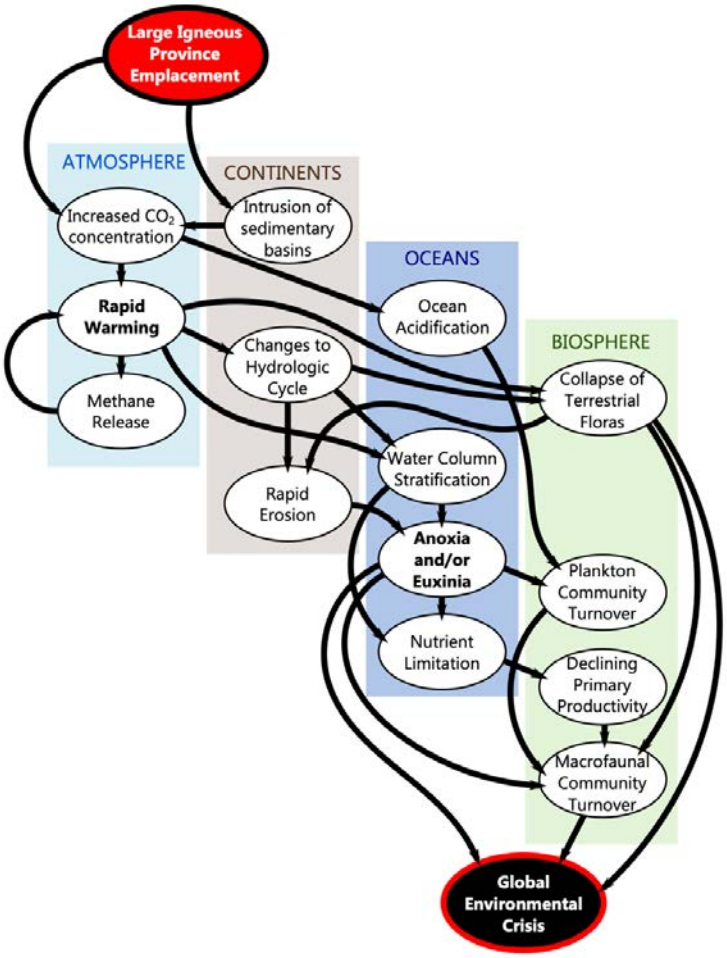


Figure 4. The deterioration of the environment consists of a cascade of destructive events. (Schöpfer et al. 2022).

The Triassic World

The Triassic began in the aftermath of the end-Permian mass extinction, EPME, and lasted from 251.9 Mya to 201.4 Mya. The geography of the Triassic was dominated by the supercontinent Pangea which was assembled during the preceding Permian and was broken up during the succeeding Jurassic (Bond and Grasby 2017, Figure 5). The Triassic was a hothouse period with low equator-to-pole temperature gradients and no ice at the poles (Kustatscher et al. 2022).

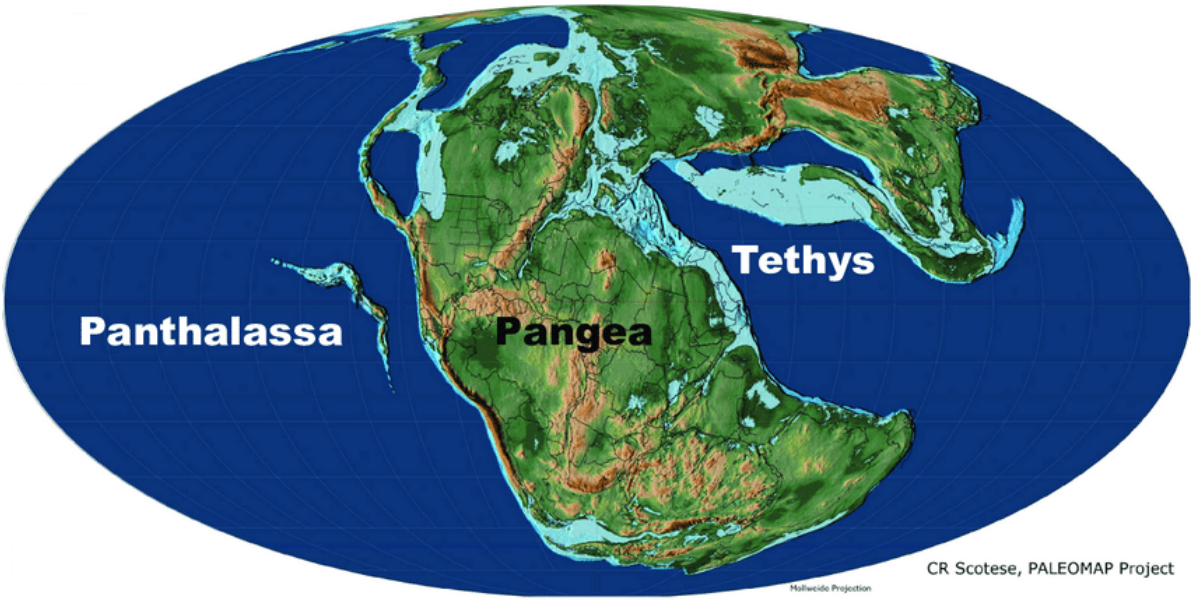


Figure 5. Topographic map of Pangea 200 Mya. From the Paleomap project.

Triassic climates

The first part of the Triassic up until 247.8 Mya was extremely hot with sea surface temperatures, SSTs, approaching 40°C, as suggested by e.g. $\delta^{18}O$ ocean temperature reconstructions from fossil carbonate shells and conodont apatite, the distribution of paleontological indicators, and climate models (Sun et al. 2012). Larger animals both at sea and on land withdrew to higher latitudes. These years are also known as the "coal gap" since no coal from that period is found which is an indication that there were no forests or coal forming environments were peat would have accumulated. There were few conifers while mosses and lycophytes were dominant (Sun et al. 2012).

Because of Pangea, the Triassic had an extremely continental climate with hot summers and cool winters (Preto et al. 2010). There were strong monsoons with heavy rainfall during the summers. The equatorial parts of Pangea and the west coast of the Tethys Ocean had a dry climate the year around, whereas the west coast of Pangea and higher latitudes of Pangea had alternating wet and dry seasons (Preto et al. 2010).

The atmospheric conditions of the Triassic were very different from those of today, the global average temperature of the Triassic was ~25°C compared to ~14°C today (Scotese et al. 2021), the level of CO_2 was ~1000 ppm compared to ~310 ppm the year 1950 (Steinthorsdottir et al. 2011), and the level of oxygen was ~15% compared to 21% today (Berner 1999).

Sea levels were low during the Triassic because there were no mid-ocean sea spreading ridges after the formation of the Pangea (Schöpfer et al. 2022).

Carnian Pluvial Episode

The Carnian Pluvial Episode, CPE, which lasted 233-232 Mya was an extinction which was followed by speciation and radiation (Dal Corso et al. 2020). It was caused by eruptions at the Wrangellia LIP on the west coast of Pangea and lead to rapid global warming, increased monsoon rains, acid rains, erosion on land, siliciclastic flux to the oceans and oceanic anoxia. After it had ended the climate returned to typical Triassic hot and dry conditions (Bond and Grasby 2017, Benton and Wu 2022). Since the EPME had been so thoroughly devastating, life in the Triassic could not be a recovery from previous life-forms. Instead, the Triassic saw the appearance and radiation of a new flora and fauna in its hot and arid environment (Figure 6). This renewal was delayed because of the "coal gap" and it was the CPE that triggered the radiations (Preto et al. 2010, Benton and Wu 2022).

Triassic animals

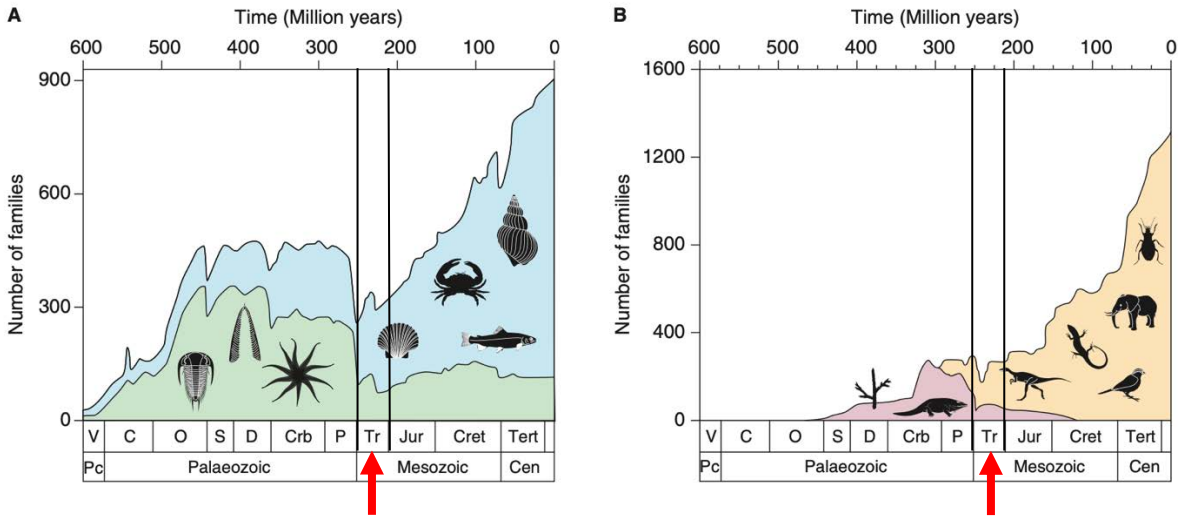


Figure 6. The Mesozoic fauna replaced the Palaeozoic fauna during the Triassic (Tr). Diagram A in the sea and diagram B on land (Benton 2016).

Synapsids, the line which ultimately would lead to the mammals, had dominated the Permian world and the most common animal in Early Triassic was the synapsid *Lystrosaurus*, a pig-sized herbivore. It existed in large herds probably because there were no predators (Modesto 2020). However, it was the reptiles that would branch out greatly during the Triassic but mainly after the CPE (Benton and Wu 2022). One branch, the archosaurs, radiated to many species, some very large, and came to dominate the Triassic landscape (Figure 7). The crocodilians started as small bipedal land animals which later became semi-aquatic. The pterosaurs took to the skies while the ichthyosaurs became fully aquatic. The pterosaurs of the Triassic had long tails. Dinosaurs were a sister group of the pterosaurs which, however, were kept low under the dominance of the archosaurs. Turtles appeared during the Late Triassic. The ancestors of crocodiles, lizards, snakes, and mammals all appeared during the Triassic (Dal Corso et al. 2020, Benton and Wu 2022).



Figure 7. Artist's rendition of a rhynchosaur, a herbivore, medium-size archosaur (Smithsonian Magazine June 21, 2023).

Meanwhile the synapsids also diversified and in Late Triassic the first mammals appeared. Both dinosaurs and synapsids changed towards walking upright with the legs under the body rather than sprawling with the legs from the sides. They both developed endothermy, which enabled a more active lifestyle, and body covering in the form of hair or feathers. These developments seem to have been accelerated by the CPE (Benton and Wu 2022). Rising oxygen levels in the Late Triassic may have aided these developments (Tanner et al. 2006). Most of modern insects such as flies, butterflies, bees, wasps and ants trace their origins back to the Triassic (Benton 2016).

The marine Palaeozoic fauna of brachiopods, rugose and tabulate corals, crinoids and graptolites went extinct in the EPME and was replaced during the Triassic by a modern fauna of bivalves, gastropods, echinoids, and bony fishes (Benton 2016). Also, reptiles like ichthyosaurs entered the ocean. Modern plankton like planktonic foraminifera, dinoflagellates, and Radiolaria appeared during the Triassic (Benton and Wu 2022). The conodonts had survived the EPME. In addition to the "coal gap" there was also a "coral gap" after the EPME of about 10 Mya before modern corals appeared (Benton 2016). Coral reefs in the ocean create habitats for other animals and plants to develop and radiate.

Triassic plants

There were two kinds of land plants during the Triassic, spore-producing plants and pollen-producing plants. Spore-producing plants were Bryophytes (mosses and lichen), Lycophytes (lycopsids), Sphenophytes (horsetails), and ferns which still exist today. Many pollen-producing plants were gymnosperms like gingkos, cycads, and conifers such as Cupressaceae, Pinaceae and the now extinct Bennettitales. Other gymnosperms were the 'seed ferns' which were broad-leaved deciduous seed plants which since have died out but some like *Dicroidium*, *Lepidopteris*, and *Thinnfeldia* were prominent during the Triassic (Vajda et al. 2023). Flowering plants and grasses did not exist at the time of the Triassic Period. During the first hot part of the Triassic, the "coal gap", there were no trees or forests (Benton and Wu 2022). Modern conifers emerged at the CPE such as pines, cypresses and yews as well as the now extinct Cheirolepidiaceae (Benton and Wu 2022, Figure 8).

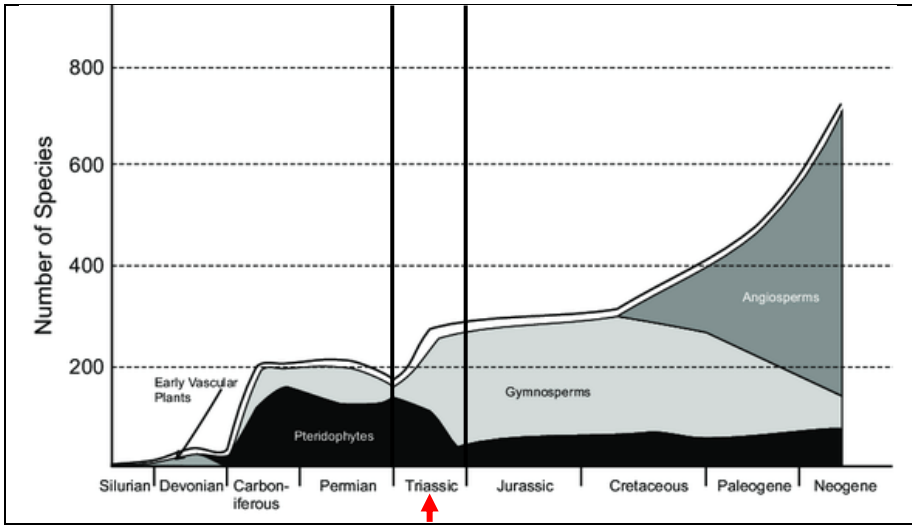


Figure 8. Dominant plant groups during the Phanerozoic, first pteridophytes (spore-producing plants), then gymnosperms and finally angiosperms (Cleal, and Cascales-Miñana 2014).

The End-Triassic mass extinction – ETME

The Triassic world was terminated by one of the 'Big Five' mass extinctions, the end-Triassic mass extinction, ETME, which occurred approximately 201.3 million years ago and was associated with the loss of 80% of species (Ernst and Youbi 2017). Careful dating has linked the ETME with a large LIP that was emplaced right in the middle of Pangea, the Central Atlantic Magmatic Province, CAMP (Schöpfer et al. 2022, Davies et al. 2017, Blackburn et al. 2013, Figure 9). The size of the CAMP is estimated to have been up to ~$7*10^6$ km^2 and the volume to between ~$2*10^6$ km^3 (Wignall 2001a) and ~$4*10^6$ km^3 (Bond and Grasby 2017). This makes the CAMP comparable with the Siberian Traps LIP of the EPME which had an estimated size of ~$7*10^6$ km^2 and volume of ~$4*10^6$ km^3 (Ivanov et al. 2013). CAMP spanned over an area of ~5,000 km north-to-south and ~2,000 km east-to-west across Pangea (Schöpfer et al. 2022) and its emplacement would lead to the opening of the North Atlantic Ocean (Ernst and Youbi 2017).

The volcanism released enormous amounts of carbon dioxide into the atmosphere as well as sulphur dioxide, halocarbons, ozone, and heavy metals, such as mercury (Lindström et al. 2019, Table 1). CO_2 levels have been calibrated using the stomatal ratio method which indicate that global temperatures may have risen by 2.5°C to 5°C (Steinthorsdottir et al. 2011, Lindström et al. 2019, Davies et al. 2017). Modelling computations show that the emplacement of sills through organic-rich sediments will suffice to produce the ~24,000 Gt carbon required (Heimdal et al. 2020). In the Amazonas 4.5 km thick sediments containing oil were intruded by CAMP sills (Heimdal et al. 2020). CAMP reached an estimated area of ~10^7 km^2 and all sediments in that area will have been burnt up or recycled (Davies et al. 2017). Another source of light carbon was intense wildfires shown by kerogen macerals (Zhang et al. 2022).

Gas	Emission (tons)
CO_2	$5.19*10^{12}$
SO_2	$2.31*10^{12}$
F	$1.11*10^{12}$
Cl	$1.58*10^{12}$
H_2O	$3.65*10^{12}$

Table 1. Total gas emissions from the CAMP (Hautmann 2021).

Lavas from the CAMP are now found on four continents and high-precision U–Pb dating of CAMP rocks show that CAMP lasted 0.8 My which means that the extinction was not a momentary event (Heimdal et al. 2020, Figures 9 and 10). During this time there were three major pulses of volcanism that brought vast influxes of light carbon, ^{12}C, which were recorded as negative carbon isotope excursions, CIEs (Bond and Grasby 2017, Algeo and Shen 2024). Those are called the Precursor, Initial, and Main CIEs or the Marshi, Spelae, and Tilmanni CIEs (Heimdal et al. 2020, Schöpfer et al. 2022). The Marshi CIE is named after the last occurrence of the Triassic index fossil *Choristoceras marshi* (Lindström et al. 2021, Hautmann 2021). The boundary between the Triassic and the Jurassic is defined by the first occurrence of the ammonite *Psiloceras spelae* but the Spelae CIE precedes that. Finally, the Tilmanni CIE is named after the Jurassic ammonite *Psiloceras tilmanni* (Lindström et al. 2019, Lindström et al. 2021).

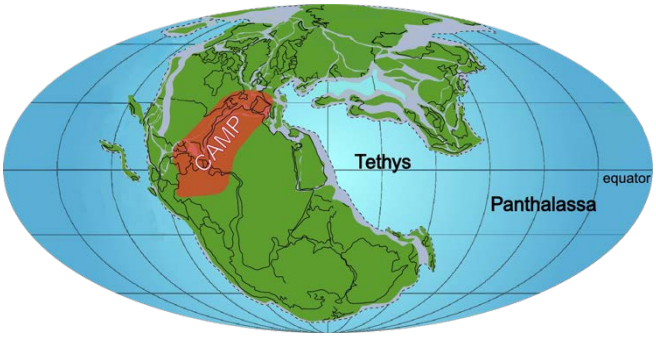


Figure 9. The Earth during the Late Triassic showing Pangea and the Central Atlantic Magmatic Province, CAMP (Lee 2023).

The Precursor CIE is linked with a transgression followed by a regression which caused the extinction in marine life (Lindström et al. 2019). During the regression large parts of the continental shelves became dry land severely restricting the habitat for marine life in shallow water (Hautman 2021). This was followed by the Initial CIE which is associated with a transgressive event drowning low lying areas thus causing stress to plants and animals on land (Lindström et al. 2019). These sea-level changes were probably connected with tectonics activities related to the CAMP and to the breaking-up of Pangea. The Initial CIE is also linked with intensified volcanism and increased global warming (Schöpfer et al. 2022). Then followed the Main CIE and a long period of $\delta^{13}C$ values lower than before the Triassic-Jurassic transition (Lindström et al 2021).

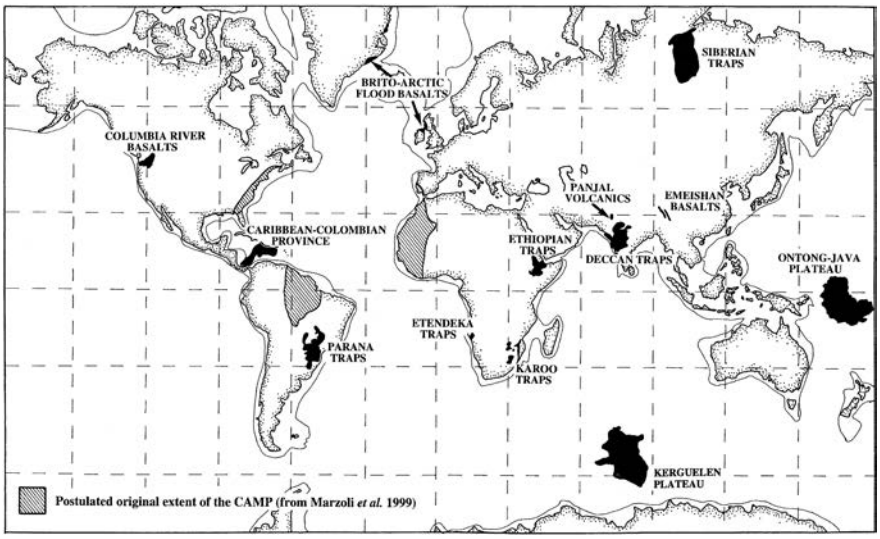


Figure 10. Hatched regions indicate present positions of CAMP lava on both sides of the Atlantic Ocean. Black shaded areas identify other large igneous provinces around the globe (Wignall 2001a).

Approximately 70 terrestrial families and 60 marine families died out at the ETME which corresponds to ~23% and ~18% families respectively becoming extinct (Wignall 2005). On land the higher temperatures led to deforestation, soil loss, deep terrestrial erosion, and sediment flux to the oceans (Schöpfer et al. 2022). The archosaurs and synapsids were entirely wiped out and this happened quite abruptly (Schöpfer et al. 2022). These were often large animals, herbivores and carnivores, which had dominated the Triassic landscape. They were ectothermic and adapted to the Triassic environment. On the other hand, dinosaurs, proto-mammals, pterosaurs and crocodilians survived (Schöpfer et al. 2022). To escape the heat animals will have moved to higher latitudes or elevations where they may have encountered volcanic winters which dinosaurs and mammals were better able to cope with since they were endothermic and had fur or feathers (Olsen et al. 2022, Benton and Wu 2022, Schöpfer et al. 2022, Figure 11).



Figure 11. *Morganucodon*, an early mammal. (©Paleocreations, Bob Nicolls)

The vegetation turnover during the ETME was more severe than could have been achieved solely by global warming. Instead pollutants such as SO_2 and polycyclic aromatic hydrocarbons, PAHs, would have exacerbated the environmental stresses (van de Schootbrugge et al. 2009). Evidence of acid rain are SO_2 damages on Ginkgoalean and Bennettitalean fossil leaf cuticles (Lindström et al. 2021, van de Schootbrugge et al. 2009). There is also an enrichment of PAHs which resulted from incomplete combustion of organic matter by intruding magma. PAHs are highly toxic to living organisms and can cause ozone depletion in the stratosphere which increases lethal UV radiation (van de Schootbrugge et al. 2009, Lindström et al. 2021). Furthermore, there were high mercury concentrations at the CIEs (Lindström et al. 2019, Zhang et al. 2022, Schöpfer et al. 2022) and kerogen macerals indicate abundant wildfires (Zhang et al. 2022).

Mass extinction in marine biota began with the Precursor CIE (Lindström et al. 2019). Higher ocean temperatures led to stratification, acidification and deep-water anoxia which struck both phytoplankton and zooplankton. 50% of marine genera and 23% of marine families went extinct (Barbacka et al. 2017). Among the marine invertebrates 40-50% of genera were lost among them almost all ammonites and nearly all genera of the scleractinian corals (Hautmann 2021). The ichthyosaurs suffered an evolutionary bottleneck, and the conodonts which had survived the EPME died out during the ETME (Schöpfer et al. 2022). In contrast, fishes endured the ETME without major faunal changes (Hautmann 2021).

Effects of the ETME on vegetation

The gymnosperm 'seed ferns' *Lepidopteris* and *Dicroidium* which had characterized the floras of the Northern and Southern Hemisphere respectively during the Triassic went extinct at the ETME (Vajda et al. 2023, van de Schootbrugge et al. 2009). Vegetation on land was affected by global warming (CO_2, CH_4), acid rain (SO_2), pollution (polycyclic aromatic hydrocarbons and heavy metals), volcanic winters and wildfires (Steinthorsdottir et al. 2011, Lindström et al. 2019, Vilas-Boas et al. 2021, Schöpfer et al. 2022, Zhang et al. 2022). Rising sea levels inundated and fragmented many coastal environments (Vilas-Boas et al. 2021, Lindström 2021) and volcanism may have thinned the ozone layer increasing the levels of potentially mutagenic UV-B radiation (Schöpfer et al. 2022). Studies of pollen and spores indicate that between 17% and 73% species went extinct while other studies indicate that 57% or even up to >95% of the macroflora did not survive the ETME (McElwain et al. 2007, Barbacka et al. 2017, Lindström 2021).

The effects of the ETME on vegetation are illustrated in Figure 12 (van de Schootbrugge et al. 2009). Time order from right to left. Conifers (Pinales) fared badly in the transition but flourished afterwards. Seed ferns (*Ricciisporites tuberculatus* and *germanicus*) decreased significantly in the transition and then became very rare or went extinct completely. Ferns (Schizaeaceae and Osmundaceae) flourished temporarily in the transition since they had a faster life cycle than trees and could spread via underground rhizomes (Lindström 2021). This is known as a fern spike (Schöpfer et al. 2022).

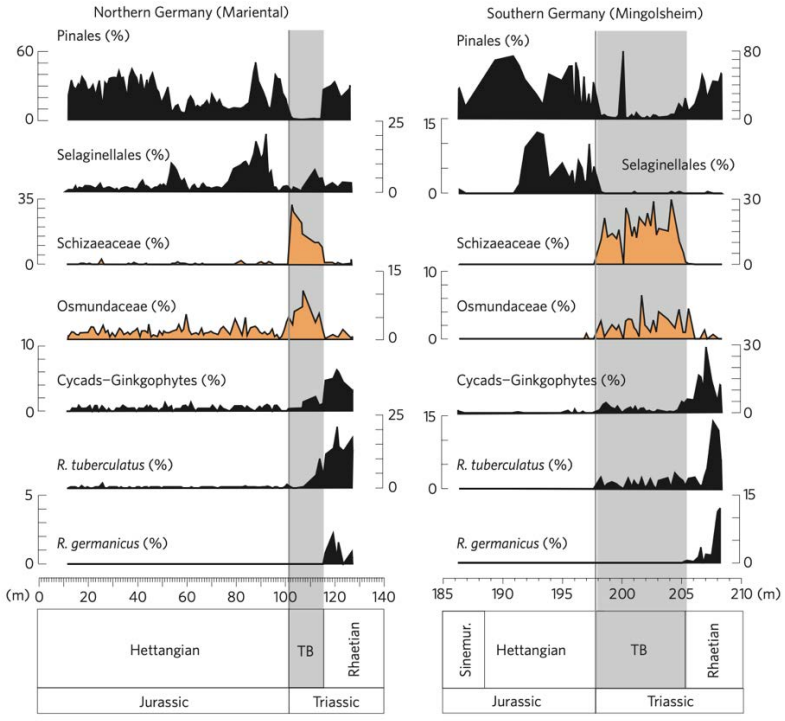


Figure 12. Changes to the vegetation across the T/J boundary as reconstructed from pollen and spores from two sites in Germany.

Pinales = Conifers.
Selaginellales = Spikemosses.
Schizaeaceae = Ferns.
Osmundaceae = Ferns.
Ricciisporites = Seed ferns.
TB = Triletes Beds, a transition layer between Triassic Rhaetian and Jurassic Hettangian. (van de Schootbrugge et al. 2009).

Researchers have observed that the devastation of the vegetation at the ETME was much greater that would be expected from global warming alone and have proposed other kill mechanisms like mercury (Lindström et al. 2019) or toxic compounds such as polycyclic aromatic hydrocarbons (van de Schootbrugge et al. 2009). The answer is probably volcanic winters as in the case of the archosaurs and dinosaurs (Olsen et al. 2022). Lengthy periods of sub-zero temperatures could be lethal for plants accustomed to the dry hot climate of the Late Triassic.

The Carnian Pluvial Episode, CPE, had been an extinction event which was followed by speciation and radiation (Dal Corso et al. 2020). Trees like Pinaceae (pines, cedars, firs), Cupressaceae (cypresses), Taxaceae (yews), and Cheirolepidiaceae which had emerged at the CPE survived the ETME whereas many seed ferns which dated back to the Early Triassic went extinct (Benton and Wu 2022).

The conifer family Cheirolepidiaceae, which produced the pollen form genus *Classopollis*, was probably related to Araucariaceae or Cupressaceae (Kürschner et al. 2013, Pocock and Jansonius 1961). Like other conifers it was affected by the extinction but became dominant in the Early Jurassic with up to >90% in many assemblages (van de Schootbrugge et al. 2009, Schöpfer et al. 2022). The Cheirolepids were drought resistant trees and shrubs resembling modern junipers (Srivastava 1976). They filled many niches later occupied by angiosperms and would in later periods become outcompeted by them (Kürschner et al. 2013, Figures 13 and 14).

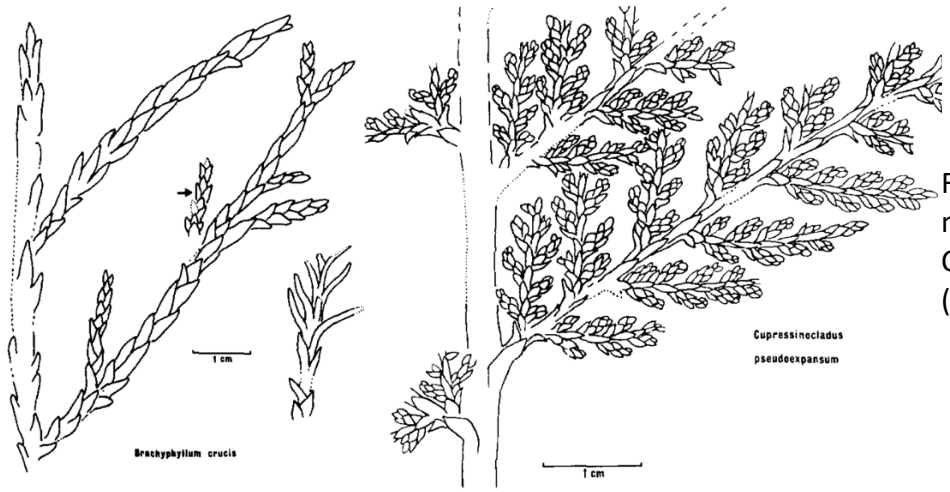


Figure 13. Shoot morphology of two Cheirolepid species (Alvin 1982).

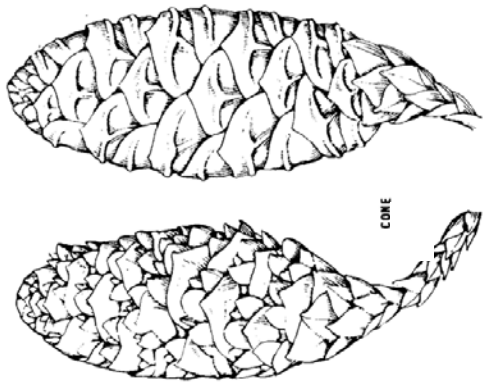


Figure 14. Cones from the Cheirolepid species *Hirmeriella muensteri* (Alvin 1982, no scale bar provided).

Effects of the ETME on pollen and spores

While evolutionary turnover and extinction of plant taxa as a whole, is one sign of extreme environmental disturbance during the ETME, other signals can be derived from the diversity and morphology of plant pollen and spores, which have an excellent fossil record. It is well known in the modern that spore and pollen morphology are really sensitive to environmental stress. This is because environmental stresses, abnormal temperatures, toxic metals or PAHs, will disturb also the reproductive parts of plants (Lindström et al. 2019). Normal sporogenesis produces 95% to 97% viable pollen or spores and 3% to 5% aberrant (abnormal), nonviable pollen or spores. If there are more than 5% aberrant pollen or spores, this is an indication of environmental stress and this applies both to current and to fossil plants (Lindström et al. 2019). When plants experience stress, like drought or changes in temperature, they often modify how much spore and pollen they produce, as well as their size, shape, and structural features of these particles. These adjustments help the plants survive and reproduce more effectively under adverse conditions. Looking at morphological changes can therefore serve as important indicators of environmental conditions, both in today and in the geological past.

Pollen are produced in groups of four grains that cluster together, called tetrads, which should separate when released (Srivastava 1976). One type of aberrancy are pollen multiples, i.e. unseparated tetrads or other combinations of more than one pollen grain (Kürschner et al. 2013, Stukins 2022, Figure 15). A further aberrancy is if a pollen multiple consists of asymmetrical (uneven-sized) grains (Baranyi et al. 2023, Kürschner et al. 2013). Dark small pollen are also aberrant (Kürschner et al. 2013, Vilas-Boas et al 2021) as well as malformed pollen (Baranyi et al. 2023, Galasso et al. 2022, Lindström et al. 2019, Kürschner et al. 2013). Giant pollen >1.5 times larger than normal might be the result of whole genome doubling (Vasilevskaya 2022).



Figure 15. Light microscope image of *Classopollis torosus* tetrads from the Early Jurassic. These unseparated tetrads consisting of more than four pollen grains were probably a response to environmental stress (van de Schootbrugge and Wignall 2016, no scale bar provided).

Examples of environmental stresses to the mother plants and to the pollen production process are global warming (Lindström et al. 2019), volcanic winters which may have occurred on higher latitudes (Schöpfer et al. 2022), UV-B radiation (Baranyi et al. 2023), acid rain (Lindström et al. 2019, Schöpfer et al. 2022, van de Schootbrugge et al. 2009), heavy metal (Hg, Cu, Cr, Cd, Pb, As) poisoning (Baranyi et al. 2023), and PAHs (Lindström et al. 2019).

It seems reasonable that warming will lead to one type of response in plants and pollen, acid rain or heavy metal poisoning to another type of response etc. Better knowledge of the types of responses would enable more detailed analyses (Benca et al. 2022). The seed fern *Lepidopteris* produced vast amounts of unseparated tetrads up to and during the ETME whereupon it went extinct (Vajda et al. 2023). This seems like the reaction to one specific type of environmental stress which eventually led to the extinction of the species.

When plants produce spores or pollen, they are highly vulnerable to environmental stress (Baranyi et al. 2023). Aberrant pollen have been observed from other extinctions such as the Late-Devonian and the end-Permian mass extinctions (Baranyi et al. 2023) and pollen are used today to estimate environmental stress at polluted locations (Galasso et al. 2022).

The genus *Classopollis* is the pollen produced by plants of the Cheirolepidiaceae family which was a conifer that occurred world-wide during the Mesozoic (Srivastava 1976, Kürschner et al. 2013). The Cheirolepids were thermophilous plants and preferred slopes and lowlands near the coast (Srivastava 1976, Alvin 1982). Thus, *Classopollis* did not go further than about 50°N paleolatitude but was frequent below about 40°N pollen with assemblages of more than 50% *Classopollis* (Alvin 1982).

Classopollis pollen grains were shaped like ellipsoids with equatorial striations and small trilete scars (Pocock and Jansonius 1961, Kürschner et al. 2013, Figure 16). The type species of the genus *Classopollis* is *Classopollis classoides* Pflug (Srivastava 1976). *Classopollis* pollen could occur as tetrads (Srivastava 1976, Figure 17) and in combinations of pollen grains of varying sizes (Kürschner et al. 2013). These are potential aberrancies and there could be a high proportion of them even at times with little environmental stress (Stukins 2022).

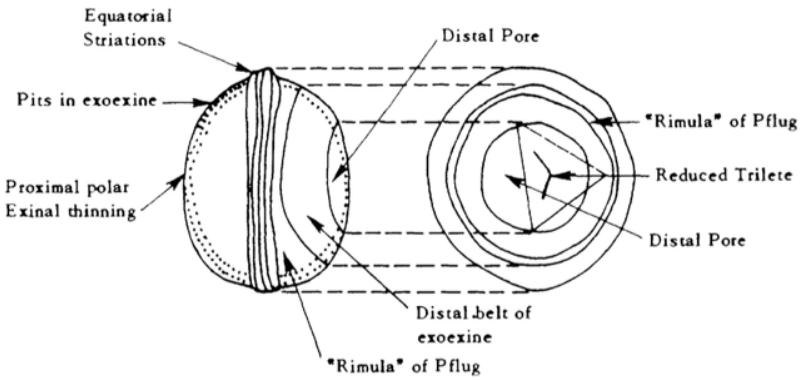


Figure 16. *Classopollis* pollen. (Pocock and Jansonius 1961)

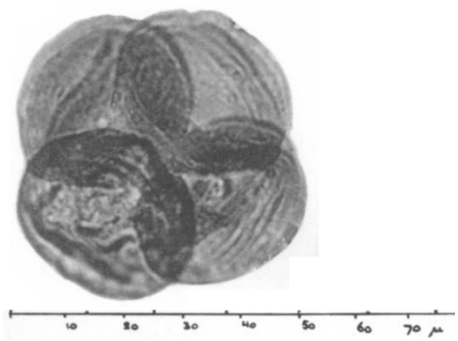


Figure 17. Light microscope image of a *Classopollis classoides* tetrad from a Canadian Jurassic sample (Pocock and Jansonius 1961)

Polyploidy

A typical plant or animal cell is diploid meaning that it has two copies of the genome (2*n*). Gametes like sperms, pollen or eggs are normally haploid with only one copy (*n*). However, unreduced gametes, which are common in many plant groups, are diploid (2*n*). Fertilization of unreduced gametes will result in polyploidy with three or more copies of the genome which also leads to larger cell size (Fox et al. 2020). Environmental stresses like high or low temperature, dry or wet climate, or salinity can cause the production of unreduced gametes which then may result in polyploidy (Fox et al. 2020). Diploid genomes may be recreated from polyploid genomes by diploidization (Fox et al. 2020). Importantly, polyploidy can result in clear differences in pollen size, morphology, and fertility in plants, which may have help reproductive success, and therefore should produce a signal in the fossil record and an indicator or environmental stress.

Polyploidy may explain the extraordinarily rapid radiation of the angiosperms. There are only 10-12 My from the earliest fossils of flowering plants to fossil records of all the major lines of angiosperms (de Bodt et al. 2005, Figure 19). There is evidence that almost all angiosperms and ferns have ancestral and recurrent polyploidy in their linages (Scholes and Paige 2015, Leitch and Leitch 2012). However, some polyploids like maize have been diploidized (Soltis and Soltis 1999).

Polyploidy is very rare among gymnosperms compared to angiosperms (Leitch and Leitch 2012) and the genome evolution among the gymnosperms is much slower than among the angiosperms (de Bodt et al. 2005, Figure 18). Angiosperms have replaced gymnosperms in many ecological niches and there is a great difference in their number of species (de Bodt et al. 2005).

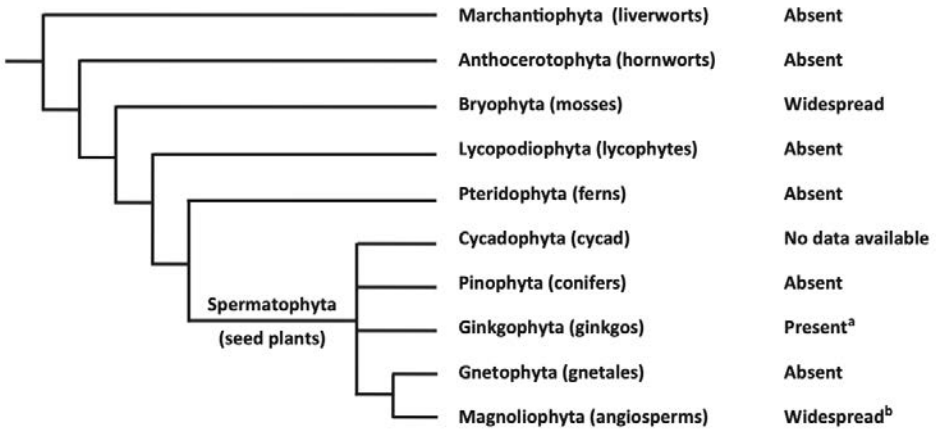


Figure 18. Occurrence of polyploidy in plants (Scholes and Paige 2015).

Polyploid species can be much more adaptable and are more tolerant to different environmental stresses. This means that polyploidy can have helped angiosperms to survive the End-Cretaceous Mass Extinction, ECME, and to radiate and expand afterwards (Fawcett et al. 2009, Fox et al. 2020).

There is evidence that most polyploidy events in angiosperm families have occurred during the last 110 My and within a short period approximately at the time of the Cretaceous–Paleogene transition which was one of the 'Big Five' mass extinctions (Fawcett et al. 2009). The polyploid plants may have had an advantage at this environmental upheaval which helped them survive and proliferate afterwards (Fawcett et al. 2009, Figure 19).

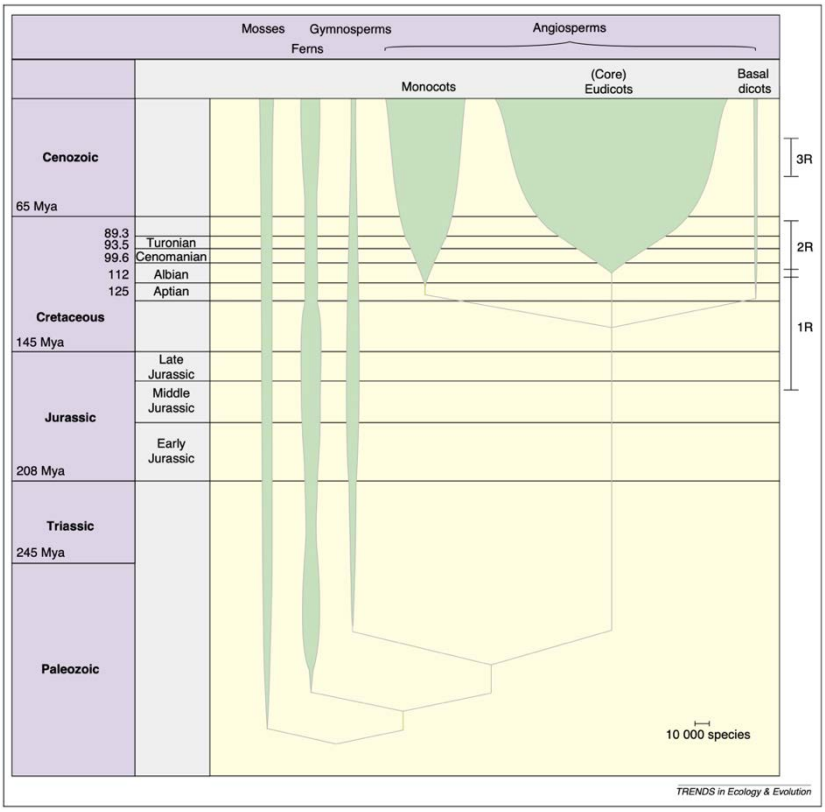


Figure 19. "Darwin's dilemma", the explosive radiation of the angiosperms (de Bodt et al. 2005).

Summary

Using this theory on the link between increased pollen and spore polyploidy, and environmental stress, this project tests for potential increased levels of aberrancy and polyploidy in *Classopollis* pollen from Pinhay Bay, UK, across the ETME as a possible indicator of environmental change at the time ca 200 million years ago.

Geological Setting

The present project was based on samples from Pinhay Bay, Devon, UK, which is located two kilometres west of the town of Lyme Regis (50° 42' 47.61 N, -2° 58' 2.5932 E, Figure 20). This area lies within the World Heritage Site Dorset and East Devon Coast.

> "The cliff exposures along the Dorset and East Devon coast provide an almost continuous sequence of rock formations spanning the Mesozoic Era, or some 185 million years of the earth's history. The area's important fossil sites and classic coastal geomorphologic features have contributed to the study of earth sciences for over 300 years." (UNESCO 2001)

This area is also known as the Jurassic Coast and is type locality for many species of reptiles, fishes, and invertebrates (Simms et al. 2004). This is where the amateur geologist Mary Anning discovered fossils of ichthyosaurs now on display at the Natural History Museum, London.



Figure 20. Map of southern England showing the location of Pinhay Bay.

The cliff face of Pinhay Bay cuts through sedimentary rock layers from Late Triassic to Early Jurassic (Cope 2016). The Triassic rocks consist of the Langport Member of the Lilstock Formation, formerly called the White Lias, while the Jurassic rocks consist of the Blue Lias Formation (Figures 21 and 22). Both have been quarried for house building and other purposes (Cope 2016).

The limestone of the Lilstock Formation was formed in a warm marine environment as is the case today at the Great Bahama Bank (Hallam 1960). During the Jurassic, Pinhay Bay was located approximately at 35°N (Cope 2016) which is at the current latitude of Algeria and Tunisia. The top bed of the Lilstock Formation is referred to as the 'Sun Bed' because of observed desiccation cracks (Wignall 2001b). There are also traces from boring and burrowing organisms as would occur if the formation rose near the sea-level or stood in a tidal environment (Hallam 1960). However, there is no conglomerate or evidence of erosion as would occur if the limestone had reached above the water (Wignall 2001b). Based on these observations it appears likely that there was a decrease in the rate of deposition at the top of the Listock Formation, but no major unconformity (Fox et al. 2022, Figure 22).



Figure 21. Photograph of the cliff face at Pinhay Bay. The red arrow points to the lithologic boundary between the Blue Lias Formation above and the Lilstock (White Lias) Formation below.

Photo Sam Slater.



Figure 22. A closeup of the lithologic boundary between the Blue Lias Formation above and the Lilstock Formation below.

Photo Sam Slater.

The Blue Lias consists of alternating shales and limestones beginning with shales indicating that the seafloor was anaerobic at the time of deposition (Cope 2016) and the depth of the water must have been at least 10 meters so that there would be no disturbance by waves (Fox et al. 2022). The abrupt change between them is the result of a transgression (Lindström et al. 2017). However, this may not be at the exact boundary between the Triassic and the Jurassic periods since that is defined by the first appearance of the ammonite *Psiloceras spelae tirolicum*, which is not present at Pinhay Bay (Schöpfer et al. 2022).

Figure 23 shows the stratigraphy across the lithologic boundary between the Lilstock Formation below the Blue Lias above. It also shows a distinct negative carbon isotope excursion from the Lilstock Formation to the Blue Lias. The Initial and the Main CIEs have been identified at St Audrie's Bay which is 56.44 km distant from Pinhay Bay and has a similar stratigraphy although with different proportions (Hesselbo et al. 2002, Figure 24). The Initial CIE, which is associated with a transgression (Lindström et al. 2019), occurred in the Lilstock Formation. It was this transgression that caused the lithologic change from limestone to shale. The Main CIE shows the change to a long period of negative $\delta^{13}C_{org}$ values towards the end of the ETME (Lindström et al. 2021).

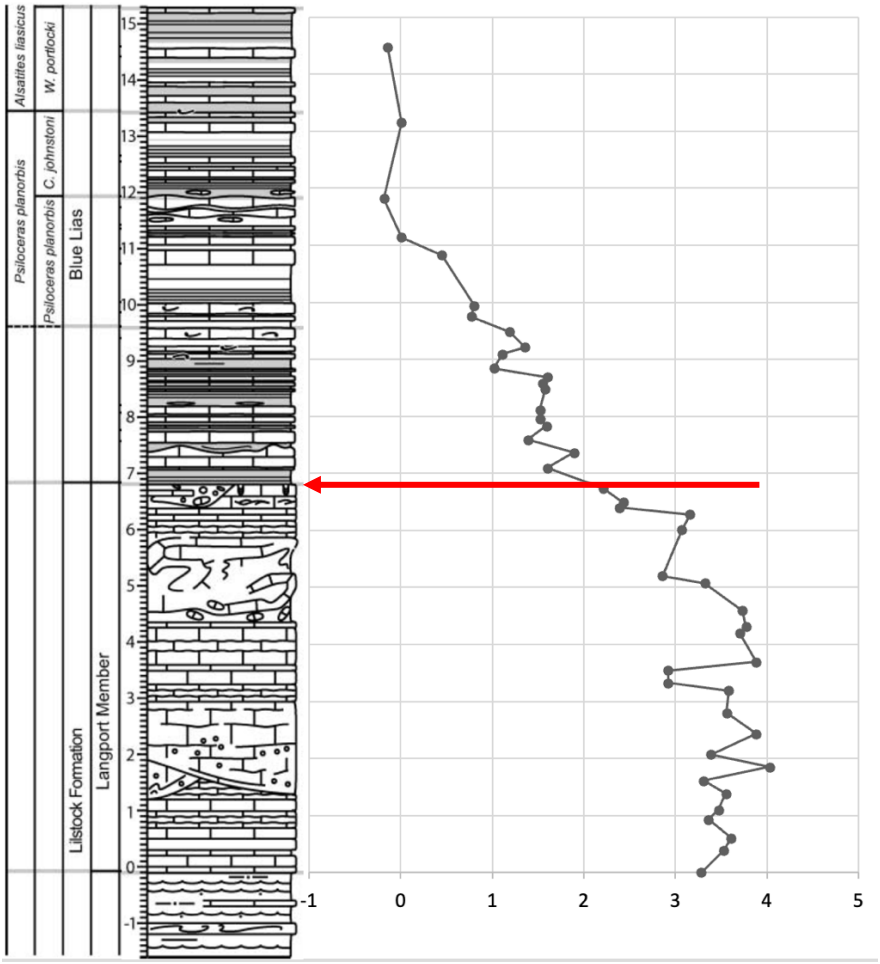


Figure 23.
Stratigraphy and $\delta^{13}C_{carb}$ data from Pinhay Bay (‰) (Korte et al. 2009).

Height above base Langport Member (m).

The red arrow points to the lithologic boundary between the Blue Lias Formation above and the Lilstock Formation below.

The columns to the left show ammonite zones and rock formations.

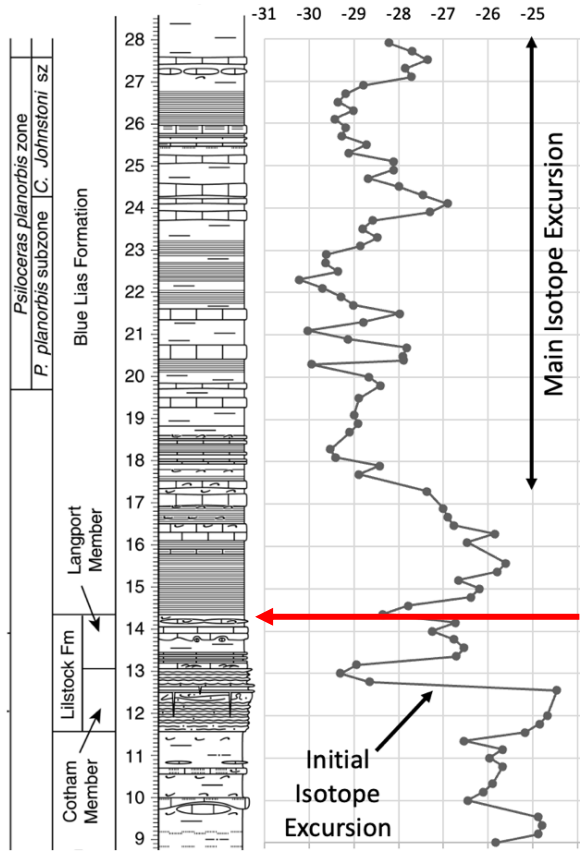


Figure 24.
Stratigraphy and $\delta^{13}C_{org}$ data from St Audrie's Bay (‰). This diagram also locates the Initial and the Main CIEs (Hesselbo et al. 2002).

Height above base Williton Member (m).

The red arrow points to the lithologic boundary between the Blue Lias Formation above and the Lilstock Formation below.

The columns to the left show ammonite zones and rock formations.

Material and methods

The material investigated consisted of 37 rock samples from Pinhay Bay which had been collected by Sam Slater in January and February 2022 at different heights of the cliff face (Figure 26). The samples in the Blue Lias are numbered 1A, 1, 2…17 from the base upwards. The samples in the Lilstock Formation are numbered 0A, 0, -1, -2…-15 from the top downwards. The average height difference between the samples is 40 cm but the samples at the boundary between Lilstock Formation and Blue Lias are only 1 cm apart (Table 2).

It is highly dangerous to climb the cliffs but since the sediments are sloping slightly from west to east it was possible to reach the different layers at beach level. This was, however, a difficult task because of the many boulders and careful attention had to be paid to the tide timetable (Cope 2016). The 37 samples were processed by standard palynological maceration techniques, using HCl and HF to isolate organic matter (e.g. Baranyi et al. 2023) by Global Geolab Ltd. The organic matter residues were pipetted on to cover slips and mounted onto glass slides, one slide from each sediment sample. From now on the samples will be referred to as slides.

The main tool for this project was an Olympus BX51 microscope fitted with an Infinity Analyze 7 camera. The camera was connected to a PC running the software package Infinity from Lumenera. The microscope was used to traverse slides horizontally from right to left and counting or measuring *Classopollis* pollen (Figure 25). The width of the traverses depended on the magnification and a traverse was always completed in full. Each traverse could be identified by its Y coordinate (mm) since there were both horizontal and vertical rulers on the specimen stage of the microscope.

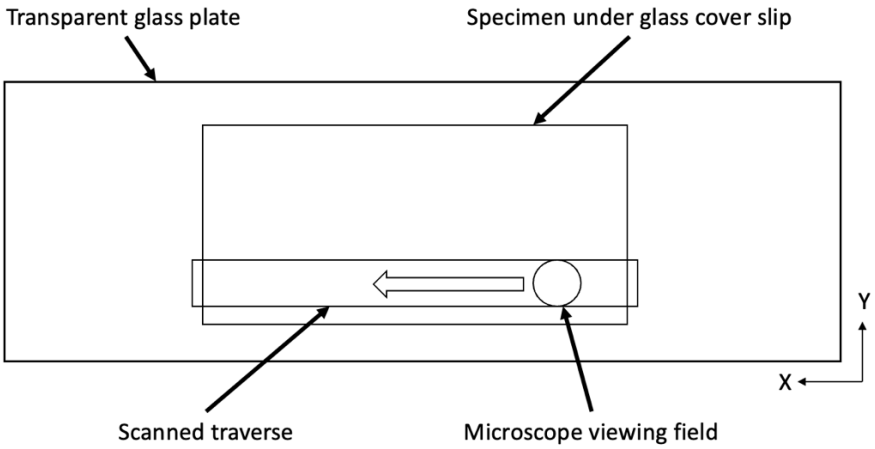


Figure 25. Scanning principles. Not to scale.

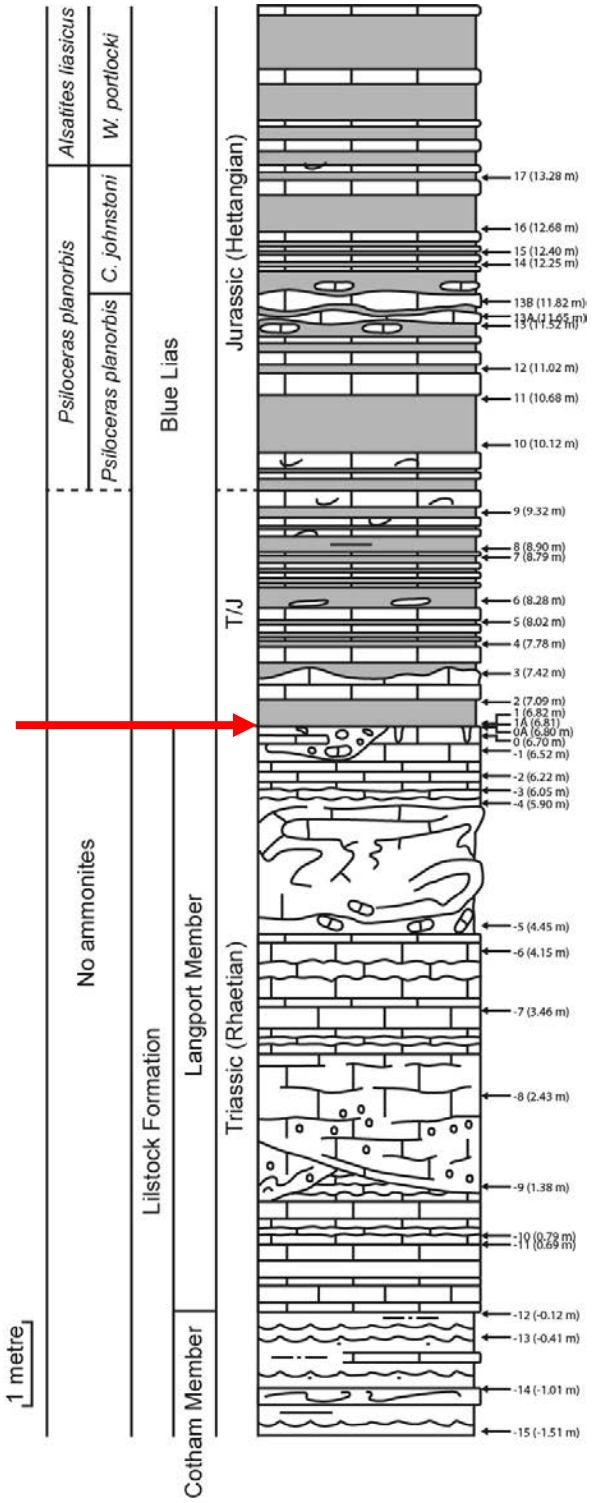
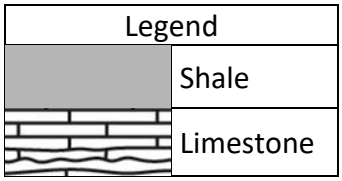


Figure 26.
Stratigraphy from Pinhay Bay showing where the different samples were collected.

The red arrow points to the lithologic boundary between the Blue Lias Formation above and the Lilstock Formation below.

Height above base Langport Member (m).

Log adapted from Korte et al. (2009).



Formation	Sample	Height (m)
Blue Lias	2	7.09
	1	6.82
	1A	6.81
Lilstock Formation	0A	6.80
	0	6.70
	-1	6.52

Table 2. Samples at the lithologic boundary.

The microscope was used to collect statistics of *Classopollis* pollen multiples, pollen grain sizes and of the symmetry of pollen multiples. The first subproject was to compute *multiplicity* over all the thirty-seven slides. This was done by traversing the slides at 20x magnification and counting the number of *Classopollis* single pollen and unseparated tetrads, i.e. double pollen, triple pollen and tetrads (Figure 27). Larger multiples might be the result of the slide preparation and were not included. At least 200 pollen were to be counted on each slide to get a statistically robust sample size.

$$\text{Multiplicity} = \frac{\text{Number of doubles, triples and tetrads}}{\text{Number of singles, doubles, triples and tetrads}} * 100$$

Singles were counted using a hand counter whereas doubles, triples and tetrads were noted directly in Excel with their X and Y coordinates. Excel was used extensively in the project for sorting, creating histograms and other computations.

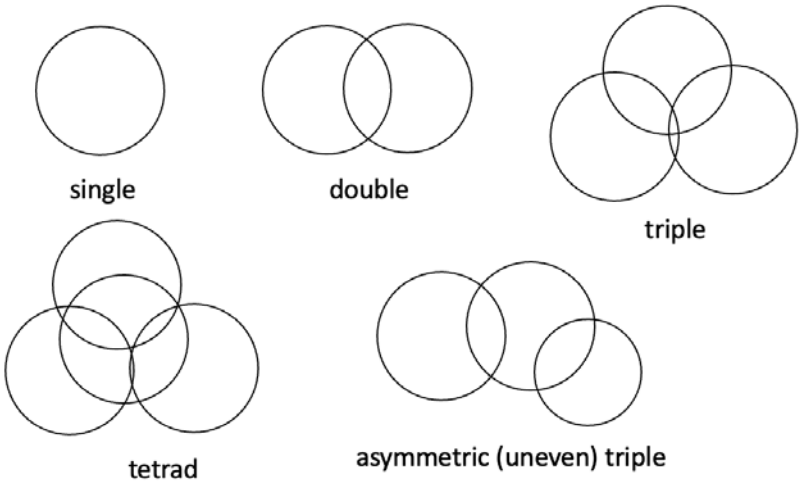


Figure 27. Examples of pollen multiple configurations.

The second subproject was to compute *size* was by traversing selected slides at 40x magnification and measuring *Classopollis* pollen grains across the longest diagonal. The project comprised computing size over ten slides and the slides -11, -7, -3, 0, 0A, 1A, 1, 4, 7, and 10 were selected since they were symmetric over the lithographic boundary. Around 200 grains were to be measured on each slide to get a statistically robust sample size. A point-and-click tool was used for measuring. The pollen grains were measured and photographed. Afterwards all photographs were checked, and the measurements were noted in Excel.

Dark small pollen were also noted since those are also regarded as aberrant (Vilas-Boas et al. 2021). The results from the size measurements were added to the multiplicity computations which was possible since different traverses had been used.

The third subproject was to measure of the evenness of pollen multiples using a novel measure invented within this project which was called *symmetry*. Several articles mention pollen multiples where the constituent pollen grains have different sizes as aberrant (Kürschner et al. 2013, Galasso et al. 2022). Symmetry was defined as the relation of the smallest pollen to the largest in a multiple expressed as a percentage:

$\text{Symmetry} = \frac{\min(a,b\ldots n)}{\max(a,b\ldots n)} * 100$, where a, b … n are the sizes of the constituent pollen grains.

Symmetry would be 100% if all pollen in a multiple are of the same size. Symmetry did not describe the full morphology of a multiple, for example three big grains and one small would

give the same result as one big grain and three small ones. However, given these limitations it presented a number that could be used for comparisons. Symmetry did not require any special measuring moment. Instead, while noting pollen sizes in Excel, it was noted whether they were part of a multiple. Thus, size data could be used for computing symmetries as well.

Results

The pollen in the samples were identified as *Classopollis torosus* after comparison with Plate III (Figure 3 and 4) and Plate V (Figure 4, 5, 6, and 8) in Vilas-Boas et al. (2021). There were only few other pollen on the slides that could be mistaken for it. On some slides there were spores, dinoflagellates and other organisms which were clearly different. Figure 31 shows pollen from ten different slides. There were more torn or folded pollen in the slides from Lilstock Formation than among those from Blue Lias. Computed pollen density/slide varied from 0.49 pollen/mm^2 to 6.66 pollen/mm^2 with an average of 2.11 pollen/mm^2

$$\text{Pollen density} = \frac{\text{Number of pollen found on the slide}}{\text{Number of traverses scanned} * \text{Length of a traverse} * \text{Width of a traverse}}$$

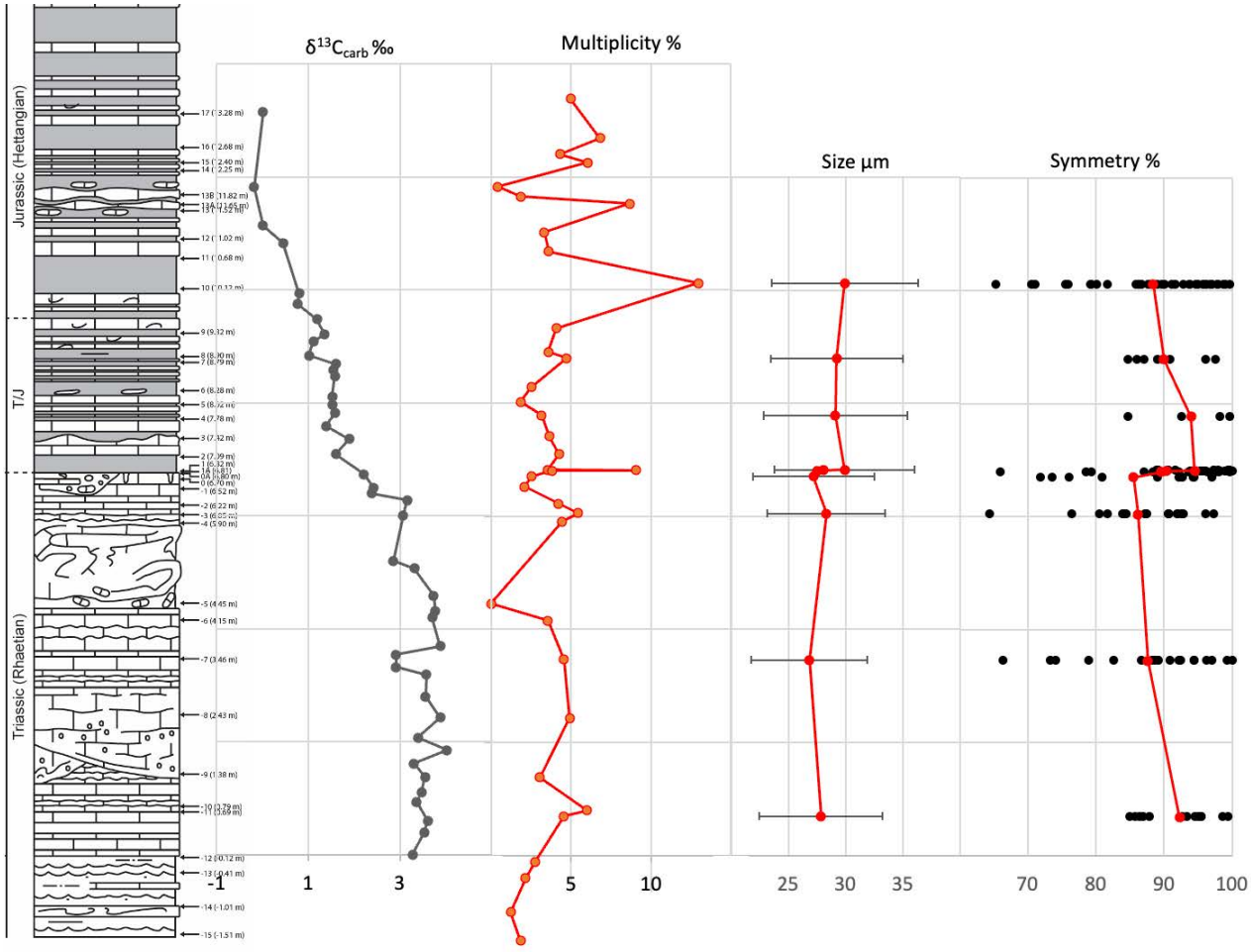


Figure 28. Compiled results from Pinhay Bay. From left to right, stratigraphy, $\delta^{13}C_{carb}$ (Korte et al. 2009), multiplicity = proportion of multiples, size shown as averages with a 95% confidence interval, symmetry shown as actual Classopollis pollen grains with averages.

Figure 28 displays the results from the subprojects. Symmetry is shown with individual data which is possible because it only includes multiples which are not too many. Size also includes singles. Table 3 is an extract from Figure 28

Slide	Height (m)	Forma-tion	Multiplicity >5%	Average size <29 µm	Symmetry <90%	>5 dark small pollen
10	10.12	Blue Lias	X		X	
7	8.79					
4	7.78					
1	6.82					
1A	6.81		X	X		X
0A	6.80	Lilstock Formation		X	X	
0	6.70			X	X	
-3	6.05		X	X	X	
-7	3.46			X	X	X
-11	0.69		X	X		

Table 3. Aberrancies and size changes from Figure 28.

Multiplicity

The results of the multiplicity computations are presented in Figure 28 and in Appendix 1. Unlike size and symmetry, multiplicity did not display an obvious trend through the studied interval. Through the Triassic Lilstock Formation multiplicity was relatively constant with an average of 3.36%. The average multiplicity in the Blue Lias was 4.66% but this was strongly influenced by three slides where multiplicity was anomalously high. Multiplicity on slide 1A at the very base of the Blue Lias appears like a "spike" which is more than two times larger than on the surrounding slides (Table 4).

Formation	Slide	Height (m)	Multiplicity (%)
Blue Lias	1	6.82	3.54
	1A	6.81	9.04
Lilstock Formation	0A	6.80	3.81
	0	6.70	2.53

Table 4. Multiplicities at the transition from Lilstock Formation to Blue Lias.

Figure 29 shows eight microscope photographs of single and multiple pollen from slide 1A. The pollen identification consists of the slide number followed by the coordinates on the slide according to England Finder notation (England).

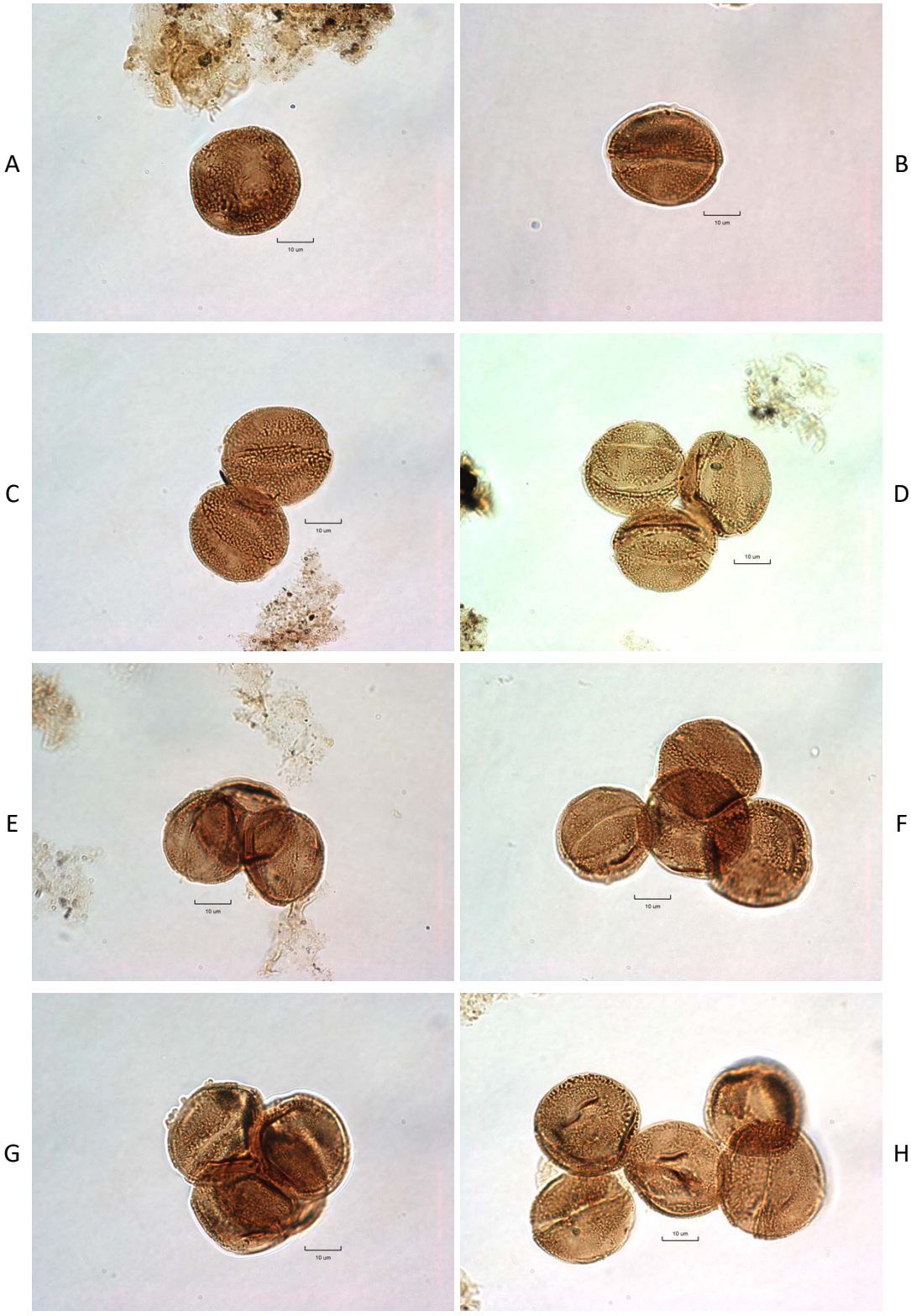


Figure 29. Light microscope images of single *Classopollis* pollen and *Classopollis* pollen multiples, from slide 1A. Scale bars = 10 µm.

A, single from above S1A_S11_100.
B, single from the side S1A_V12_1_100.
C, double S1A_U14_3_100.
D, triple S1A_H26_1_100.
E, triple S1A-Q14_2_100.
F, tetrad S1A_E25_1_100.
G, tetrad S1A_E8_3_100.
H, quintuple S1A_T16_100.

Pollen grain size

The results from measuring pollen sizes are shown in Figure 28 and Table 5. This also lists the number of dark small pollen found.

Slide	Height (m)	Pollen grains measured	Traverses covered	Average size (µm)	Standard deviation (µm)	Large pollen ≥35.0 (µm)	Large pollen ≥38.0 (µm)	Dark small pollen
10	10.12	399	6	29.93	3.20	16	1	3
7	8.79	196	6	29.23	2.88	3	0	0
4	7.78	175	10	29.10	3.14	6	1	0
1	6.82	243	3	29.91	3.06	6	0	0
1A	6.81	590	3	28.11	2.23	0	0	7
0A	6.80	357	6	27.52	3.33	6	1	2
0	6.70	333	2	27.20	2.66	0	0	1
-3	6.05	303	3	28.33	2.57	0	0	3
-7	3.46	349	3	26.83	2.52	1	0	8
-11	0.69	423	9	27.85	2.69	4	0	0
	Total	3368	51					

Table 5. Results from measuring pollen grain sizes (longest diagonal).

Figure 30 shows examples of how the measurements were carried out and Figure 31 shows photographs of sample pollen from each of the slides where size measurements were carried out, i.e. the slides 10, 7, 4, 1, 1A, 0A, 0, -3, -7, and -11.



Figure 30. Light microscope images of *Classopollis* pollen on slide 1A from the measurement session. One single and one triple.

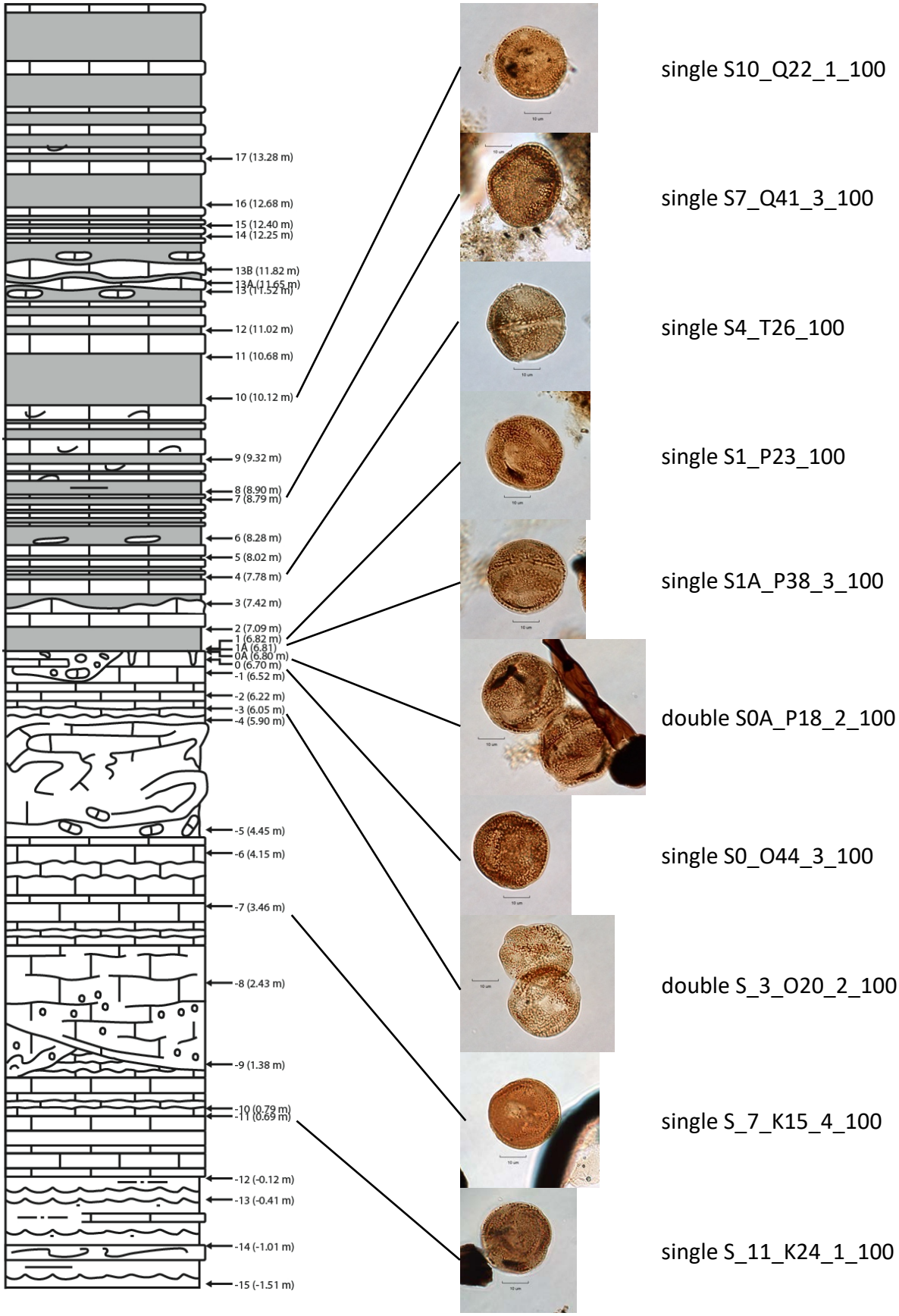


Figure 31. Light microscope images of *Classopollis* pollen from the slides 10, 7, 4, 1, 1A, 0A, 0, -3, -7, and -11. Scale bars = 10 µm.

Pollen multiple symmetry

The results from computing average pollen multiple symmetries are shown in Figure 28 and Table 6. Figure 32 shows an example of an asymmetric pollen multiple. The average *symmetry* was 88.6% for the slides in the Lilstock Formation and 91.5% for the slides in the Blue Lias. The average symmetry increased from 86.2% in slide 0 from the Lilstock Formation to 94.3% in slide 1 from the Blue Lias. Table 6 also shows that the few higher multiples were concentrated to slides 1A and 10. Slide 1A at the base of the Blue Lias is noticeable since it also represented a "multiplicity spike".

Slide	Average symmetry (%)							
	Doubles	Triples	Tetrads	Fives	Sixes	Eights	Tens	All
10	92.2	86.6	85.2				65.3	88.8
7	93.1	87.6	86.0					90.2
4	96.8	84.7						93.8
1	95.1	89.2						94.3
1A	93.2	91.4	87.4	76.4	88.3	86.3	85.7	90.5
0A	91.7		65.9					89.8
0	84.4	93.3						86.2
-3	90.7	79.9	85.0					86.8
-7	90.3	73.3	66.3					88.1
-11	91.8	95.1	95.5					92.3

Table 6. Results from calculating average symmetries.

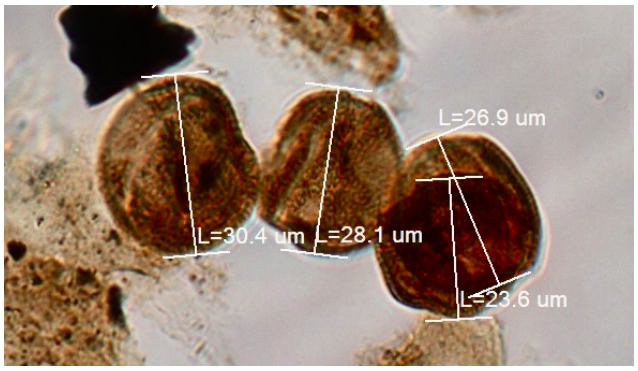


Figure 32. Light microscope image of an asymmetric (uneven) *Classopollis* pollen multiple on slide 1A.

Smallest pollen grain = 23.6 µm.
Largest pollen grain = 30.4 µm.
Symmetry = 77.63%.

Dark Small Pollen

Twenty-four dark small pollen grains were photographed while measuring pollen *size*. This means that they were 0.7% of all pollen measured (Table 5). Almost all dark small pollen were found on slides 1A and -7. Figure 33 shows different pollen multiples which contain dark small pollen.

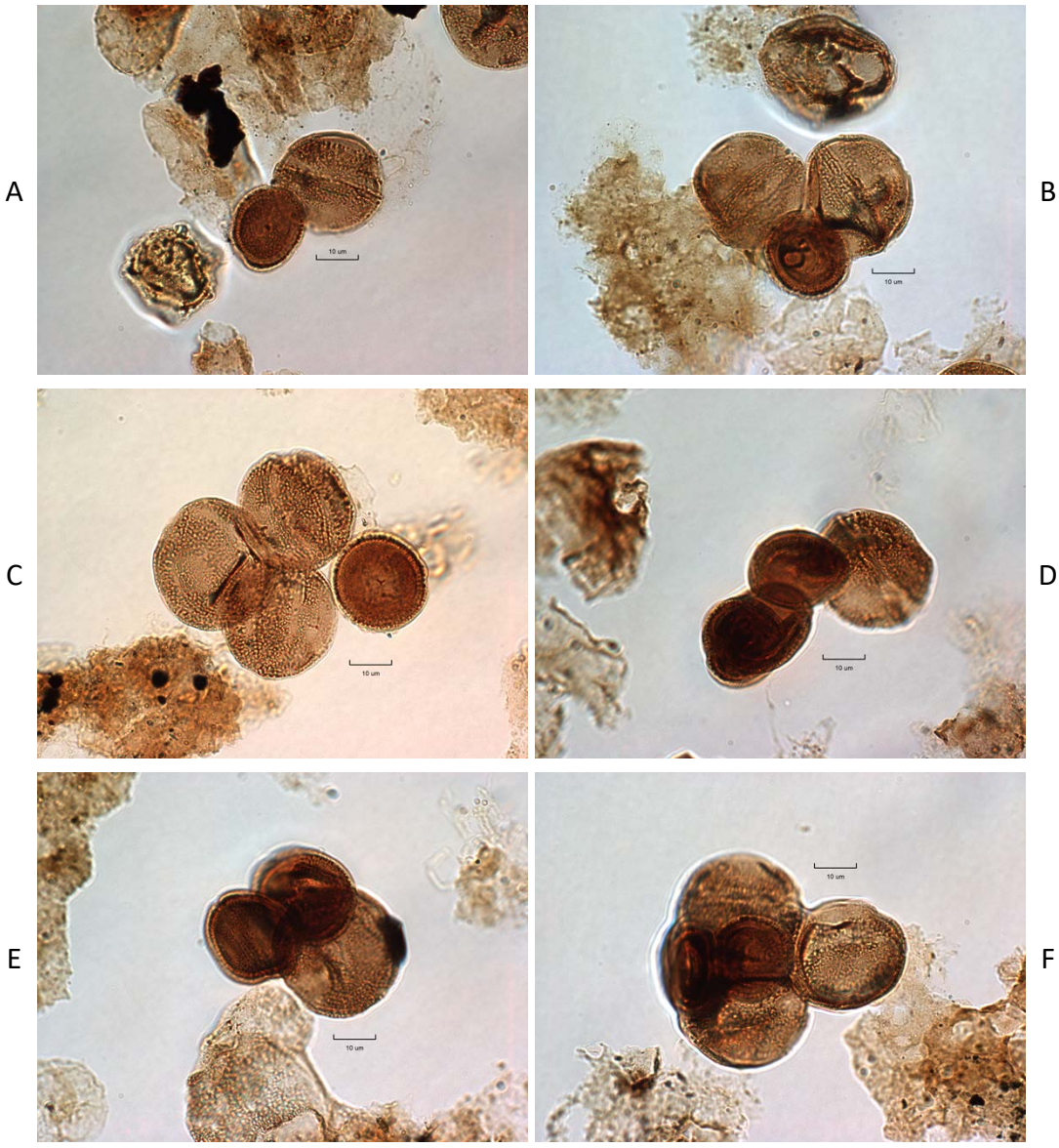


Figure 33. Light microscope images of probable aberrant *Classopollis* pollen multiples with dark small pollen from slide 1A. Scale bars = 10 µm.

A, double S1A_L11_100.
B, triple S1A_H24_100.
C, tetrad S1A_T35_3_100.
D, tetrad S1A_O20_4_100.
E, triple S1A_N41_100.
F, quintuple S1A_W25_3_100.

Discussion

Multiplicity

Multiplicity remained relatively constant throughout the tested interval except for the values of the slides 1A, 10 and 13 where multiplicity was aberrantly high (Figure 28 and 34). The histogram in Figure 34 clearly shows how those stood out from the other slides. If those three slides were excluded, the average multiplicity at the Blue Lias became 3.68%, instead of 4.66%, which was near the average multiplicity of 3.36% at the Lilstock Formation and well below 5% which is the limit of being aberrant (Lindström et al. 2019).

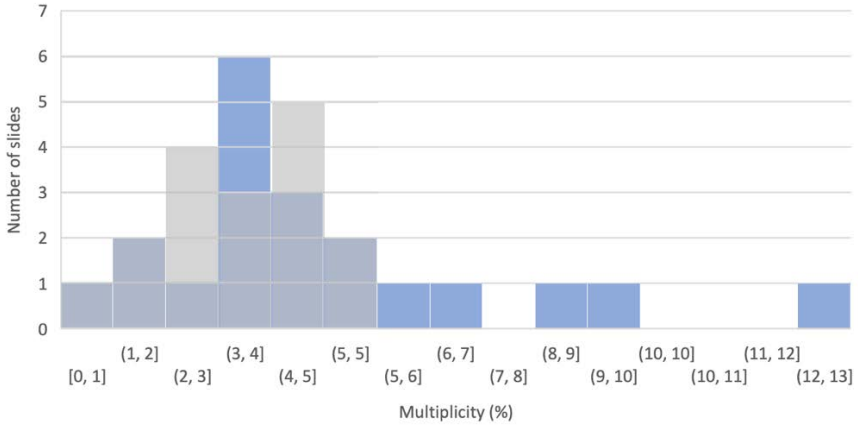


Figure 34. Histogram of the multiplicity of the slides from the Blue Lias and the Lilstock Formation.

Blue = Blue Lias.
Grey = Lilstock Formation.
Bluegrey = Overlap.

Slide 1A with an average multiplicity of 9.04% at the very base of the Blue Lias represented a "multiplicity spike" (Table 4). Slide 1A comes from the time when the transgression occurred and may have been the result of the Initial CIE (Lindström et al. 2019). It has also unusually many different multiples, doubles, triples, tetrads, quintuples etc (Table 6). In addition, slide 1A occurs at a point in time with a drop in $\delta^{13}C$ (Korte et al. 2009, Figure 28). Slide 10 had an average multiplicity of 12.96% which is the largest value of all the slides. It occurred at the base of a thick layer of shale which might indicate yet a further transgression (Figure 26). Both slide 13 with an average multiplicity of 8.65% and slide 10 occurred at times with a drop in $\delta^{13}C$ (Korte et al. 2009, Figure 28). More samples might reveal if they too represented "multiplicity spikes". Slides 10 and 13 may have been the result of the Main CIE which was long period of negative $\delta^{13}C_{org}$ values (Lindström et al. 2021).

The conclusion is that multiplicity remained relatively stable throughout the tested interval except for the values of three slides from the Blue Lias. This shows that the Cheirolepids responded to episodes of extreme environmental stress but also that they survived, recovered and continued thriving.

Pollen grain size

The average grain size of *Classopollis* pollen increased by 1.6 µm from the Lilstock Formation to the Blue Lias (Table 7). This is also visible in figure 28.

Formation	Slides	No of pollen	Averages (µm)
Blue Lias	1A, 1, 4, 7, 10	1603	29.1
Lilstock Formation	-11, -7, -3, 0, 0A	1765	27.5

Table 7. Average pollen sizes.

A histogram of the datasets from Blue Lias and Lilstock Formation pollen grain sizes is shown in figure 35. A statistical T test gave the answer $P = 1.32e^{-52} < 0.05$ which indicates that the datasets were statistically significantly different (Excel student T test).

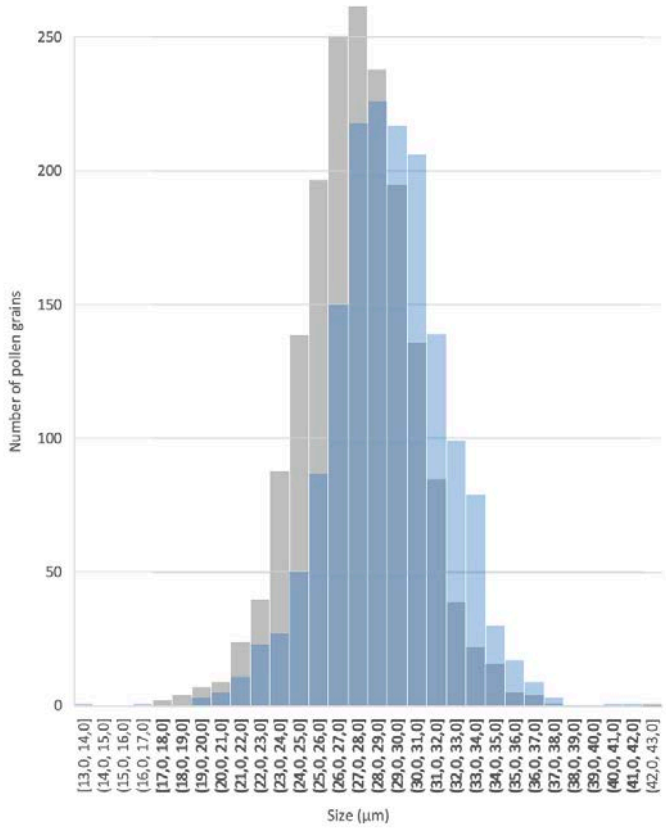


Figure 35.

Histogram of the number of pollen grains at different sizes from the Blue Lias and the Lilstock Formation.

Grey = Lilstock Formation.
Light blue = Blue Lias.
Dark blue = Overlap.

Lilstock Formation and Blue Lias represented distinct depositional environments, shallow marine for the Lilstock, and deeper marine for the Blue Lias (Fox et al. 2022, Wignall 2001b). The limestone of Lilstock Formation was laid down in very shallow water whereas the water when the shale of Blue Lias was deposited was tens of meters deep due to the transgression following the Initial CIE (Lindström et al. 2017, Fox et al. 2022). Tens of meters of water depth vertically correspond to hundreds of meters of inundation horizontally especially in flat ground and on low-lying meadows. Thus, pollen deposited in the Blue Lias would have travelled several hundred meters further from land than pollen deposited in the Lilstock Formation. This would have selected for buoyant (both in air and water) pollen in

the deeper marine sediments (i.e. the Blue Lias). This pattern is widely documented within the field of palynology and is known as the 'Neves effect' (Chaloner 1958). This means that care must be taken when such pollen are analysed since those may reflect depositional rather than environmental circumstances from the time that they were laid down.

Pollen multiple symmetry and dark small pollen

The average *symmetry* increased from 88.6% to 91.5% from the Lilstock Formation to the Blue Lias. This was probably a reflection of the same depositional circumstances as for grain *size* in that the 'Neves effect' selected for large and symmetric (even) pollen multiples.

Asymmetric (uneven) pollen multiples are characterized by at least one constituent pollen grain being markedly smaller than the others because of stunted growth due to environmental stress. Today *ecological palynology* uses pollen of woody and herbaceous species as a bioindicator of the level of environmental pollution and the presence of mutagens (Vasilevskaya 2022). A study of the conifer *Pinus sylvestris* in the impact area of the Severonickel metallurgical plant at Murmansk showed that the proportion of viable pollen was 2-3 times lower than in the control samples (Vasilevskaya 2022). Many pollen grains were small, immature or degenerated. Pollen size is proposed to be used as a bioindicator of air pollution (Vasilevskaya 2022).

Slides 0A, 0, and -7 have low *multiplicity* but those few pollen multiples also have low *symmetry* (Table 3). Benca et al. (2022) suggest that different aberrancies could identify which environmental stresses had affected the parent plant. In the case of these three slides, there would have been a low environmental stress to cause *multiplicity* but a high environmental stress to cause small pollen grains and thus uneven multiples. A possible explanation from ecological palynology is that these slides represented times of high environmental pollution by polycyclic aromatic hydrocarbons and heavy metals such as mercury.

Dark small pollen were probably another example where normal development has been impaired (according to this reasoning) because of pollution. Dark small pollen seem to have occurred only when there were other aberrancies as well (Table 3). Most dark small pollen appeared on slide 1A and slide -7 (Table 5).

Van de Schootbrugge et al. (2009) described a 'dark zone' as a stratigraphic indicator of the End Triassic which has been observed at sites in Germany, Denmark, and Sweden. Spores and pollen are much darker in the upper Triassic sediment layers than below which they proposed was caused by sulphuric acid from the CAMP. No such 'dark zone' was observed among the samples from Pinhay Bay (Figure 31). However, Vermeer (2023) suggested instead that the dark colours were caused by high temperatures from forest fires. It might be that the deposition in water prevented the creation of a 'dark zone' of pollen at Pinhay Bay.

Stukins (2022) studied *Classopollis* from a site in Argentina which goes back to the quiescent and cool Bajocian stage, 170.9 Mya to168.2 Mya, during the mid-Jurassic and found that between 2.8% and 8.4% of tetrads had at least one reduced/aborted pollen grain. These tetrads would have been typical uneven multiples. This means that some level of *asymmetry* was always present. In this project the highest average symmetry was 94.3% on slide 1 (Table 6).

Potter Canyon

A comparison was made with the data from Potter Canyon in Figure 4 in the article by Kürschner et al. (2013). The article data were downloaded from the supplements and converted to Excel. *Classopollis* pollen grains from Potter Canyon were on the average 3.87 µm larger than those from Pinhay Bay, Table 8.

	Pinhay Bay	Potter Canyon
Number of pollen grains in study	3368	1400
Smallest pollen grain (µm)	12.8	23.96
Largest pollen grain (µm)	42.2	51.62
Average pollen grain size (µm)	28.27	32.14
Histogram skew	1.142	-0.00859

Table 8. Comparing the results from Pinhay Bay and Potter Canyon.

A histogram of the datasets from Pinhay Bay and Potter Canyon is shown in figure 36. A statistical T test gave the answer $P = 6.19e^{-302} < 0.05$ which indicates that the datasets were statistically significantly different (Excel student T test).

In the histogram from Potter Canyon there is a tail of eleven *Classopollis* which are larger than 40.0 µm and the largest is 51.62 µm. It is among those large pollen that Kürschner et al. (2013) proposed that genome doubling might be found.

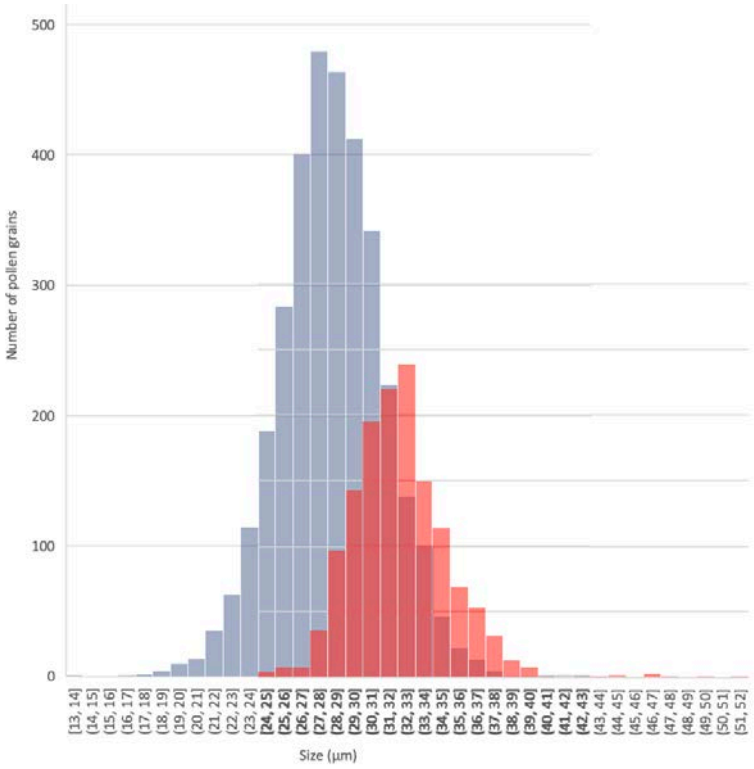


Figure 36.

Histograms of the number of pollen at different sizes from Pinhay Bay and from Potter Canyon.

Grey = Pinhay Bay.
Light red = Potter Canyon.
Deep red = Overlap.

The histogram from Potter Canyon corresponds to Figure 4 in Kürschner et al. (2013).

The sandstone at Potter Canyon, which is of the same age as the limestone of Lilstock Formation at Pinhay Bay, was too coarse grained to have preserved any pollen. Above this there is grey to black shale indicating that the transgression had occurred. This corresponds to the Blue Lias at Pinhay Bay and contains pollen (Figure 37).

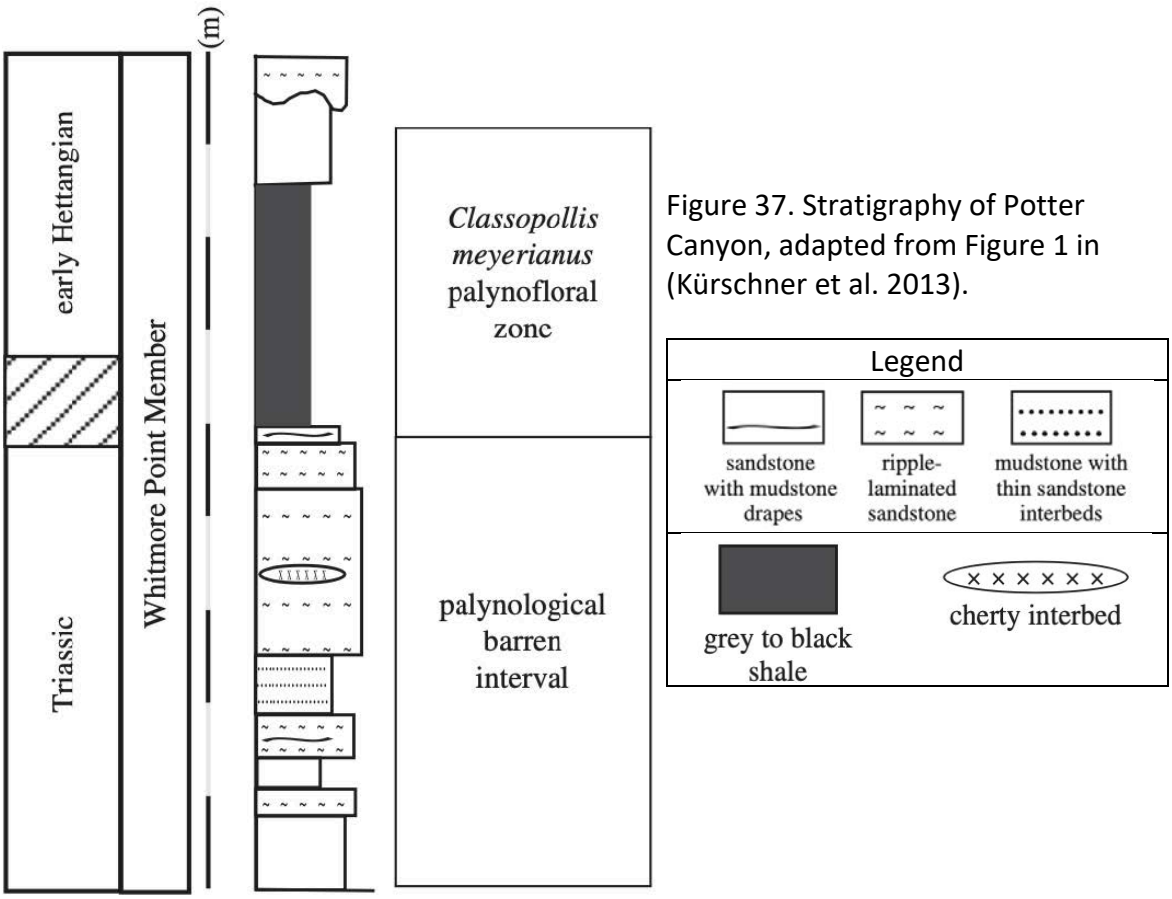


Figure 37. Stratigraphy of Potter Canyon, adapted from Figure 1 in (Kürschner et al. 2013).

Thus, the data from Potter Canyon ought to be compared with the data from the Blue Lias rather than with the whole data set from Pinhay Bay. Pollen grains from Potter Canyon were on the average 3 µm larger than those from the Blue Lias (32.14 µm as against 29.1 µm). The pollen at Potter Canyon was *Classopollis meyerianus* (Kürschner et al. 2013) while the pollen at Pinhay Bay has been identified as *Classopollis torosus*. *Classopollis meyerianus* pollen had smooth surfaces and no striations (Plate II (Figure 9) and Plate V (Figure 7) in Vilas-Boas et al. 2021, Srivastava 1976, Figure 38).



Figure 38. Light microscope images of *Classopollis meyerianus*. Scale bars = 20 µm. **(**Kürschner et al. 2013)

Potter Canyon lay on the west coast of Pangea and Pinhay Bay lay in an archipelago in an epicontinental sea on the east side of Pangea (Figure 1 in Lindström 2021). Not only were they positioned on either side of Pangea but also on either side of the CAMP which implies that wind directions were important. At their latitude the predominant surface winds were from the north-east to the south-west (Ikeda et al. 2015). This means that Potter Canyon may have suffered more by heat, smoke and poisonous substances from the CAMP than Pinhay Bay which instead may have received fresh air from the Tethys Ocean (Figure 39).

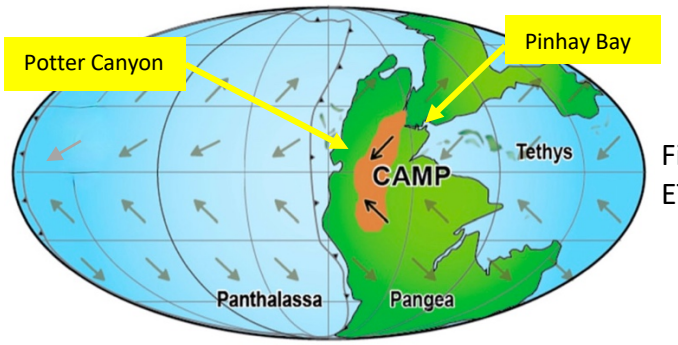


Figure 39. Surface wind directions at the ETME (Ikeda et al. 2015).

Polyploidy

Polyploid pollen are larger than normal haploid pollen (Fox et al. 2020) and since the genomic content increases stepwise, (*n*), (2*n*), (3*n*) …, pollen size also increases by discrete increments. For *Classopollis meyerianus* those polyploid increments were 45, 49, 55 and 60 µm (Kürschner et al. 2013). Figure 36 shows histograms of the number of pollen at different sizes from Potter Canyon and Pinhay Bay and for Potter Canyon there is a tail of eleven pollen grains larger than 40.0 µm which are outside the standard distribution. This tail is enlarged in Figure 40 and the polyploid pollen sizes are indicated. This histogram illustrates the hypothesis of large polyploid *Classopollis* pollen at the time of the ETME.

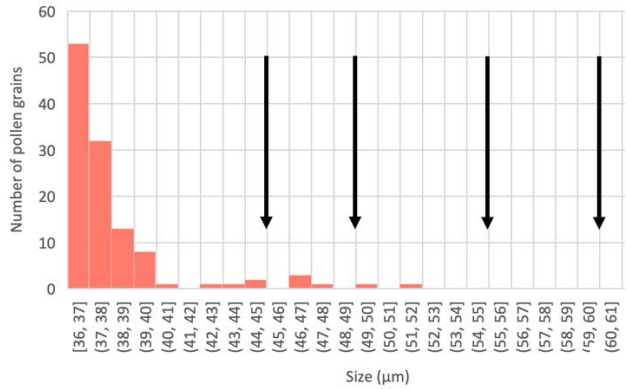


Figure 40. Histogram of the number of pollen at different sizes from 36 µm upwards from Potter Canyon.

The arrows indicate discrete multiplications of pollen volume (2*n*), (3*n*) etc.

Since *Classopollis torosus* was on the average 3 µm smaller than *Classopollis meyerianus* the polyploid pollen grain sizes can be hypothesized to have been 42, 46, 52 and 57 µm. Those are displayed in Figure 41 which shows the upper end of the histogram for Pinhay Bay. The two largest pollen, which were at the end of the standard distribution, were 41.7 and 42.2 µm. This was also the size of diploid pollen, making them ambiguous, but there was no tail of anomalously large pollen beyond them.

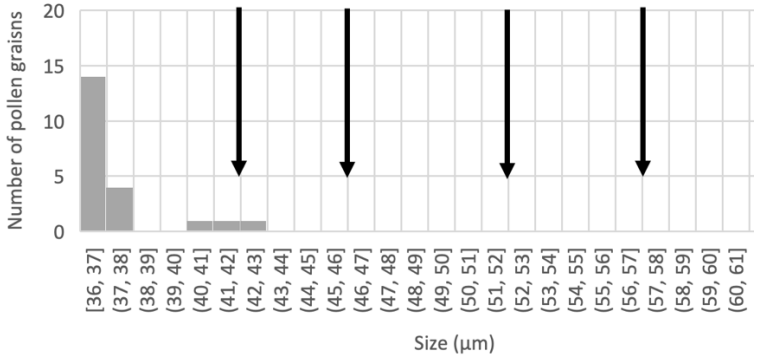


Figure 41. Histogram of the number of pollen at different sizes from 36 µm upwards from Pinhay Bay.

The arrows indicate discrete multiplications of pollen volume (2*n*), (3*n*) etc.

Environmental stress like high or low temperatures can lead to the production of unreduced (2*n*) gametes (Fox et al. 2020). The study of the conifer *Pinus sylvestris* in the impact area of the Severonickel metallurgical plant at Murmansk found not only small and degenerated pollen but also giant pollen, 1.5 times larger than normal, which were interpreted as diploid (Vasilevskaya 2022). It is estimated that ~0.5% of all gametes in angiosperms are unreduced in a normal situation (Arrigo and Barker 2012). Thus, diploid pollen are not too uncommon. Polyploid species are rarer and despite their importance in angiosperm radiation (de Bodt et al. 2005), it turns out that they have high extinction rates and that only few of them survive permanently (Arrigo and Barker 2012).

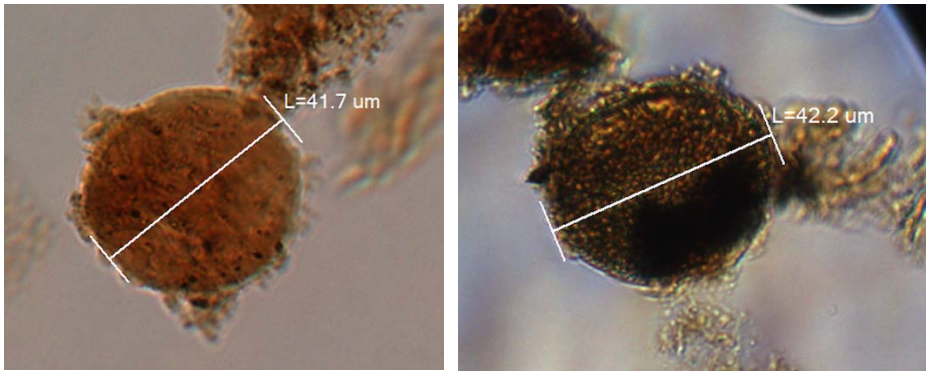


Figure 42. Light microscope images of the two largest *Classopollis* pollen among the samples from Pinhay Bay. 41.7 µm on slide 10 and 42.2 µm on slide 0A.

Classopollis resilience

An alternative hypothesis to why the Cheirolepids survived the ETME could be that they were able to endure volcanic winters. Olsen at al. (2022) argue that the ETME on land was caused by volcanic winters which may have been more than 10 years long. Large archosaurs which were ectothermic and lacked insulating hair or feathers died out while dinosaurs and early mammals survived. As mentioned in the section “Effects of the ETME on Vegetation” an analogue development may have occurred among plants. Seed ferns accustomed to the Triassic climate went extinct at the ETME whereas conifers like Cheirolepidiaceae and Pinacaea which appeared during the CPE survived and flourished during the Jurassic (Cirilli 2010, Dal Corso et al. 2020, Benton and Wu 2022).

Conclusions

Research questions

1. Did any aberrancies occur among the *Classopollis* pollen from the Pinhay Bay site, UK, during the Triassic-Jurassic transition period?

2. Is there any indication of whole genome doubling among the *Classopollis* pollen from the Pinhay Bay site, UK, during this period?

The answer to the first question is that some aberrancies were observed. Seven discontinuous samples of the 37 samples in this study had more than 5% pollen multiples. Size changes as a reaction to transgressions caused by the volcanism were observed as well as some uneven pollen multiples and some dark small pollen. In sum, the Cheirolepids, which produced the *Classopollis* pollen, showed moderate reaction to the environmental stresses of this transition period but carried through and continued flourishing afterwards.

The answer to the second question is that no unambiguous cases of whole genome doubling were observed. The largest pollen grains found in this study were too small to stand out from the normal distribution. In sum, the location at Pinhay Bay may have been a less exposed location during this transition period than Potter Canyon. The fact that there were different Cheirolepid species at those locations may also have been important.

Future work

This project found indications that uneven-sized pollen multiples and small pollen are linked to poisonous pollution and by default that pollen multiples could be linked to warming. This could be investigated further because if it is correct then it can help in the interpretation of pollen found in sediments from mass extinctions.

Animals such as mammals and dinosaurs as well as plants such as the Pinaceae and the Cheirolepidiaceae originated or diversified during the CPE and then went on to survive the ETME (Dal Corso et al. 2020, Olsen at al. 2022). The mechanisms behind this could be further investigated. A hypothesis is that there occurred volcanic winters during the CPE as well since it seems to have been conducive to the radiation of very hardy species.

Acknowledgements

My acknowledgements are above all due to my supervisor Sam Slater, researcher at the Department of Palaeobiology at the Museum of Natural History in Stockholm. Sam had collected the samples and prepared the slides. He has also taken the photographs from Pinhay Bay.

I am also indebted to Helen Coxall, Professor of Marine Micropalaeontology at the Department of Geological Sciences at Stockholm University, and to Timothy Topper, researcher at the Department of Palaeobiology at the Museum of Natural History, for allowing me to carry out my Master project at the Museum of Natural History as part of my geoscience studies at Stockholm University.

References

Algeo, T. J., and Shen, J. 2024. *Theory and classification of mass extinction causation*. National Science Review, vol 11, issue 1.

Alvin, K. L. 1982. *Cheirolepidiaceae: Biology, structure, and paleoecology*. Review of Palaeobotany and Palynology, issue 37, pp. 71-98.

Arrigo, N., and Barker, M. S. 2012. *Rarely successful polyploids and their legacy in plant genomes*. Current Opinion in Plant Biology 2012, 15:140–146

Baranyi, V., Jin, X., Dal Corso, J., Shi, Z., Grasby, S. E., and Kemp, D. B. 2023. *Collapse of terrestrial ecosystems linked to heavy metal poisoning during the Toarcian oceanic anoxic event*. GEOLOGY, vol. 51, no. 7.

Barbacka, M., Pacyna, G., Kocsis, Á. T., Jarzynka, A., Ziaja, J., and Bodor, E. 2017. *Changes in terrestrial floras at the Triassic-Jurassic Boundary in Europe*. Palaeogeography, Palaeo-climatology, Palaeoecology, issue 480, pp 80–93.

Barnosky, A. D., Matzke, N., Tomiya, S., Wogan, G. O. U., Swartz, B., Quental, T. B., Marshall, C., McGuire, J. L., Lindsey, E. L., Maguire, K. C., Mersey, B., and Ferrer, E. A. 2011. *Has the Earth's sixth mass extinction already arrived?* Nature, vol 471.

Benca, J. P., Duijnstee, I. A. P., and Looy, C. V. 2022. *Fossilized pollen malformations as indicators of past environmental stress and meiotic disruption: insights from modern conifers*. Paleobiology, 48(4), 2022, pp. 677–710.

Benton, M. J. 2016. *The Triassic*. Current Biology, vol 26, pp. 1214-1218.

Benton, M. J., and Wu, F. 2022. *Triassic Revolution*. Frontiers in Earth Science, vol 22, article 899541.

Berner, R. A. 1999. *Atmospheric oxygen over Phanerozoic time*. PNAS, vol 96, pp. 10955–10957.

Blackburn, T. J., Olsen, P. E., Bowring, S. A., McLean, N. M., Kent, D. V., Puffer, J., McHone, G., Rasbury, E. T., and Et-Touhami, M. 2013. *Zircon U-Pb Geochronology Links the End-Triassic Extinction with the Central Atlantic Magmatic Province*. Science, vol 340.

Bond, D. P. G, and Grasby, S. E. 2017. *On the causes of mass extinctions*. Palaeogeography, Palaeoclimatology, Palaeoecology 478, pp. 3–29.

Chaloner, W. G. 1958. *The Carboniferous upland flora*. Geological Magazine. 95(3), pp. 261–262.

Cirilli, S. 2010. *Upper Triassic lowermost Jurassic palynology and palynostratigraphy: a review*. Geological Society, London, Special Publications, vol 334, pp. 285-314.

Cleal, C. J. and Cascales-Miñana, B. 2014. *Composition and dynamics of the great Phanerozoic Evolutionary Floras. Lethaia*, doi: 10.1111/let.12070.

Cope, J. C. W. 2016. *Geology of the Dorset Coast*. The Geologists' Association. 2nd edition.

Dal Corso, J., Bernardi, M., Sun, Y., Song, H., Seyfullah, L. J., Preto, N., Gianolla, P., Ruffell, A., Kustatscher, E., Roghi, G., Merico, A., Hohn, S., Schmidt, A. R., Marzoli, A., Newton, R. J., Wignall, P. B., and Benton, M. J. 2020. *Extinction and dawn of the modern world in the Carnian (Late Triassic)*. Science Advances, vol 6.

Davies, J. H. F. L., Marzoli, A., Bertrand, H., Youbi, N., Ernesto, M., and Schaltegger, U. 2017. *End-Triassic mass extinction started by intrusive CAMP activity*. Nature Communications, DOI: 10.1038/ncomms15596.

de Bodt, S., Maere, S., and van de Peer, Y. 2005. *Genome duplication and the origin of angiosperms*. TRENDS in Ecology and Evolution, vol 20, no 11.

(England) The England Finder https://www.agarscientific.com/the-england-finder

Ernst, R. E., and Youbi, N. 2017. *How Large Igneous Provinces affect global climate, sometimes cause mass extinctions, and represent natural markers in the geological record*. Palaeogeography, Palaeoclimatology, Palaeoecology 478, pp. 30–52.

Fawcett, J. A., Maerea, S., and de Peera, Y. V. 2009. *Plants with double genomes might have had a better chance to survive the Cretaceous–Tertiary extinction event*. PNAS, vol 106, no 14, pp. 5737–5742.

Fox, D. T., Soltis, D. E., Soltis, P. S., Ashman, T.-L., and van de Peer, Y. 2020. *Polyploidy: A Biological Force from Cells to Ecosystems*. Trends in Cell Biology, vol 30, no 9.

Fox, C. P., Whiteside, J. H., Olsen, P. E., and Grice, K. 2022. *Flame out! End-Triassic mass extinction polycyclic aromatic hydrocarbons reflect more than just fire*. Earth and Planetary Science Letters 584 (2022) 117418.

Galasso, F., Feist-Burkhardt, S., and Schneebeli-Hermann, E. 2022. *Do spores herald the Toarcian Oceanic Anoxic Event?* Review of Palaeobotany and Palynology 306 (2022) 104748

Hallam, A. 1960. *The White Lias of the Devon coast*. Proceedings of the Geologists' Association, vol 71, issue 1, pp 47-60.

Hautmann, M. 2021. *Extinction: End-Triassic Mass Extinction*. eLS, vol 2, issue 7, pp. 1–15, doi: 10.1002/9780470015902.a0029378.

Heimdal, T. H., Jones, M. T., and Svensen, H. H. 2020. *Thermogenic carbon release from the Central Atlantic magmatic province caused major end-Triassic carbon cycle perturbations*. PNAS, vol. 117, no. 22.

Hesselbo, S. P., Robinson, S. A., Surlyk, F., and Piasecki, S. 2002. *Terrestrial and marine extinction at the Triassic-Jurassic boundary synchronized with major carbon-cycle perturbation: A link to initiation of massive volcanism?* Geology, March 2002.

Ikeda, M., Hori, R. S., Okada, Y., and Nakada, R. 2015. *Volcanism and deep-ocean acidification across the end-Triassic extinction event*. Palaeogeography, Palaeoclimatology, Palaeoecology, vol 440, pp. 725–733.

Ivanov, A. V., He, H., Yan, L., Ryabov, V. V., Shevko, A. Y., Palesskii, S. V., and Nikolaeva, I. V. 2013. *Siberian Traps large igneous province: Evidence for two flood basalt pulses around the Permo-Triassic boundary and in the Middle Triassic, and contemporaneous granitic magmatism*. Earth-Science Reviews, vol 122, pp. 58–76.

Korte, C., Hesselbo, S. P., Jenkyns, H. C., Rickaby, R. E. M., and Spötl, C. 2009. *Palaeo-environmental significance of carbon- and oxygen-isotope stratigraphy of marine Triassic −Jurassic boundary sections in SW Britain.*
Journal of the Geological Society 2009, vol. 166, pp. 431-445.

Kustatscher, E., Ash, S. R., Karasev, E., Pott, C., Vajda, V., Yu, J., and McLoughlin, S. 2022. Flora of the Late Triassic. In: Tanner, L. H. (ed.), *The Late Triassic World*, Topics in Geobiology 46, Springer International Publishing AG.

Kürschner, W. M., Batenburg, S. J., and Mander, L. 2013. *Aberrant Classopollis pollen reveals evidence for unreduced (2n) pollen in the conifer family Cheirolepidiaceae during the Triassic–Jurassic transition.* Proceedings of the Royal Society B 280: 20131708.

Lee, H. 2023. *How the world of the end-Triassic extinction was similar to today—and how it differed*. Ars Technica, WIRED Media Group.

Leitch, A. R., and Leitch, I. J. 2012. *Ecological and genetic factors linked to contrasting genome dynamics in seed plants*. New Phytologist, vol 194, pp. 629–646.

Lindström, S., van de Schootbrugge, B., Hansen, K. H., Pedersen, G. K., Alsen, P., Thibault, N., Dybkjær, K., Bjerrum, C. J., and Nielsen, L. H. 2017. *A new correlation of Triassic–Jurassic boundary successions in NW Europe, Nevada and Peru, and the Central Atlantic Magmatic Province: A time-line for the end-Triassic mass extinction*. Palaeogeography, Palaeoclimatology, Palaeoecology, issue 478, pp. 80–102.

Lindström, S., Sanei, H., van de Schootbrugge, B., Pedersen, G. K., Lesher, C. E., Tegner, C., Heunisch, C., Dybkjær, K., and Outridge, P. M. 2019. *Volcanic mercury and mutagenesis in land plants during the end-Triassic mass extinction*. Science Advances, no. 5, 2019.

Lindström, S. 2021. *Two-phased Mass Rarity and Extinction in Land Plants During the End-Triassic Climate Crisis.* Frontiers in Earth Science, November 2021, vol 9.

Lindström, S., Callegaro, S., Davies, J., Tegner, C., van de Schootbrugge, B., Pedersen, G. K., Youbi, N., Sanei, H., and Marzoli, A. 2021. *Tracing volcanic emissions from the Central Atlantic Magmatic Province in the sedimentary record*. Earth-Science Reviews, vol 212.

McElwain, J. C., Popa, M. E., Hesselbo, S. P., Haworth, M., and Surlyk, F. 2007. *Macroecological responses of terrestrial vegetation to climatic and atmospheric change across the Triassic/Jurassic boundary in East Greenland*. Paleobiology, vol 33, pp. 547-573.

Metcalfe, I., and Isozaki, Y. 2009. *Current perspectives on the Permian–Triassic boundary and end-Permian mass extinction: Preface*. Journal of Asian Earth Sciences, vol 36, pp. 407–412

Modesto, S. P. 2020. *The Disaster Taxon Lystrosaurus: A Paleontological Myth*. Frontiers in Earth Science, vol 8, article 610463

Olsen, P., Sha, J., Fang, Y., Chang, C., Whiteside, J. H., Kinney, S., Sues, H.-D., Kent, D., Schaller, M., and Vajda, V. 2022. *Arctic ice and the ecological rise of the dinosaurs*. Science Advances, 8, eabo6342

Pocock, S. J., and Jansonius, J. 1961. *The Pollen Genus Classopollis Pflug. 1953.* Micropaleontology, vol. 7, no. 4, pp. 439-449.

Preto, N., Kustatscher, E., and Wignall, P. B. 2010. *Triassic climates — State of the art and perspectives.* Palaeogeography, Palaeoclimatology, Palaeoecology, vol 290, pp. 1–10.

Routley, M. 2020. *Incredible Map of Pangea with Modern-Day Borders*. Visual Capitalist.

Scholes, D. R., and Paige, K. N. 2015. *Plasticity in ploidy: a generalized response to stress*. Trends in Plant Science, vol 20, no 3.

Schöpfer, S. D., Algeo, T. J. van de Schootbrugge, B., and Whiteside, J. H. 2022. *The Triassic–Jurassic transition – A review of environmental change at the dawn of modern life.* Earth-Science Reviews 232 (2022) 104099.

Scotese, C. R., Song, H., Mills, B. J. W., and van der Meer, D. G. 2021. *Phanerozoic paleotemperatures: The earth's changing climate during the last 540 million years*. Earth-Science Reviews, vol 215. https://doi.org/10.1016/j.earscirev.2021.103503

Sepkoski, J. J. 1986. Phanerozoic Overview of Mass Extinction. In: Raup, D. M. and Jablonski, D., eds: *Patterns and Processes in the History of Life*. Springer Verlag, pp. 277-294.

Simms, M.J., Chidlaw, N., Morton, N., and Page, K.N. 2004. *British Lower Jurassic Stratigraphy*. Geological Conservation Review Series No. 30. Joint Nature Conservation Committee, Peterborough, ISBN 1 86 107 495 6.

Simms, M. J. 2007. *Uniquely extensive soft-sediment deformation in the Rhaetian of the UK: Evidence for earthquake or impact*? Palaeogeography, Palaeoclimatology, Palaeoecology, vol 244, pp. 407–423.

Soltis, D. E., and Soltis, P. S. 1999. *Polyploidy: recurrent formation and genome evolution*. TREE, vol 14, no 9.

Srivastava, S. K. 1976. *The fossil pollen genus Classopollis*. Lethaia, nr 9, pp. 437-457.

Steinthorsdottir, M., Jeram, A. J., McElwain, J. C. 2011. *Extremely elevated CO_2 concentrations at the Triassic/Jurassic boundary.* Palaeogeography, Palaeoclimatology, Palaeoecology, issue 308, pp. 418–432.

Stukins, S. 2022. *Is Aberrancy a reliable indicator for major paleoclimatic disturbance?* PALAOIS, vol. 37, pp. 145–149.

Sun, Y., Joachimski, M. M., Wignall, P. B., Yan, C., Chen, Y., Jiang, H., Wang, L., and Lai, X. 2012. *Lethally Hot Temperatures During the Early Triassic Greenhouse*. Science, vol 338, pp. 366-370.

Tanner, L. H., Lucas, S. G., and Zeigler, K. E. 2006. Rising oxygen levels in the Late Triassic: Geological and evolutionary evidence. In: Harris et al., eds., *The Triassic-Jurassic Terrestrial Transition*. New Mexico Museum of Natural History and Science Bulletin 37.

Thibodeau, A. M., Ritterbush, K., Yager, J. A., West, A. J., Ibarra, Y., Bottjer, D. J., Berelson, W. M., Bergquist, B. A., and Corsetti, F. A. 2016. *Mercury anomalies and the timing of biotic recovery following the end-Triassic mass extinction*. Nature Communications, doi: 10.1038/ncomms11147

UNESCO 2001. *World Heritage Committee Inscribes 31 New Sites on the World Heritage List*. https://whc.unesco.org/en/news/143/

Vajda, V., McLoughlin, S., Slater, S. M., Gustafsson, O., and Rasmusson, A. G. 2023. *The 'seed-fern' Lepidopteris mass-produced the abnormal pollen Ricciisporites during the end-Triassic biotic crisis*. Palaeogeography, Palaeoclimatology, Palaeoecology, nr 627.

van de Schootbrugge, B., Quan, T. M., Lindström, S., Püttmann, W., Heunisch, C., Pross, J., Fiebig, J., Petschick, R., Röhling, H.-G., Richoz, S., Rosenthal, Y., and Falkowski, P. G. 2009. *Floral changes across the Triassic/Jurassic boundary linked to flood basalt volcanism.* Nature Geoscience, vol. 2, doi: 10.1038/NGEO577.

van de Schootbrugge, B. and Wignall, P. B. 2016. *A tale of two extinctions: converging end-Permian and end-Triassic scenarios*. Geological Magazine, issue 153, pp. 332-354.

Vasilevskaya, N. 2022. *Pollution of the Environment and Pollen: A Review*. Stresses, Issue 2, pp. 515–530. https://doi.org/10.3390/stresses2040035

Vermeer, J. 2023. *The cause of terrestrial biodiversity turnover during the Triassic-Jurassic boundary using spore darkness as a climate proxy.* Master Thesis. Utrecht University

Vilas-Boas, M., Pereira, Z., Cirilli, S., Duarte, L. V., and Fernandes, P. 2021. *New data on the palynology of the Triassic–Jurassic boundary of the Silves Group, Lusitanian Basin, Portugal*. Review of Palaeobotany and Palynology 290 (2021) 104426.

Wignall, P. B. 2001a. *Large igneous provinces and mass extinctions*. Earth-Science Reviews, no 53, pp. 1–33.

Wignall, P. B. 2001b. *Sedimentology of the Triassic-Jurassic boundary beds in Pinhay Bay (Devon, SW England).* Proceedings of the Geologists' Association, vol 112, issue 4, pp 349-360.

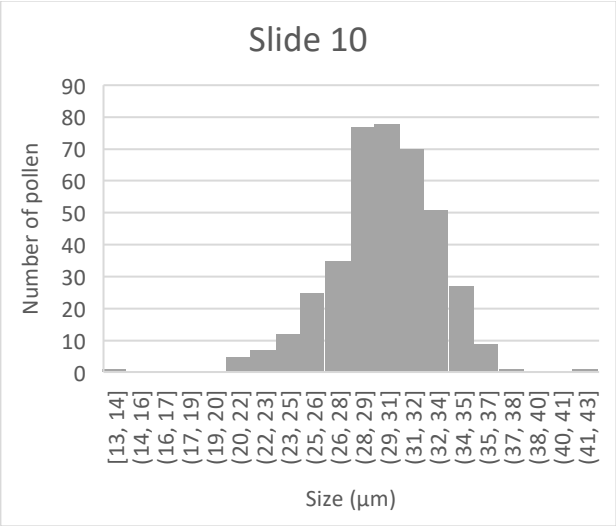
Wignall, P. B. 2005. *The End Triassic Mass Extinction*. © 2005 John Wiley & Sons, Ltd.

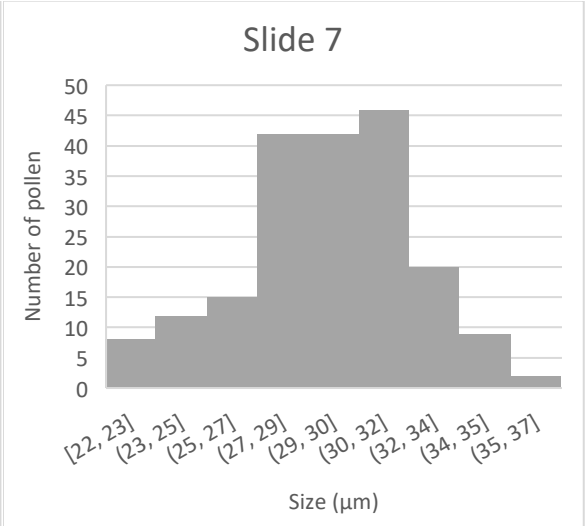
Zhang, P., Lu, J., Yang, M., Bond, D. P. G., Greene, S. E., Liu, L., Zhang, Y., Wang, Y., Wang, Z., Li, S., Shao, L., and Hilton, J. 2022. *Volcanically Induced Environmental and Floral Changes Across the Triassic-Jurassic (T-J) Transition*. Frontiers in Ecology and Evolution, vol. 10, article 853404.

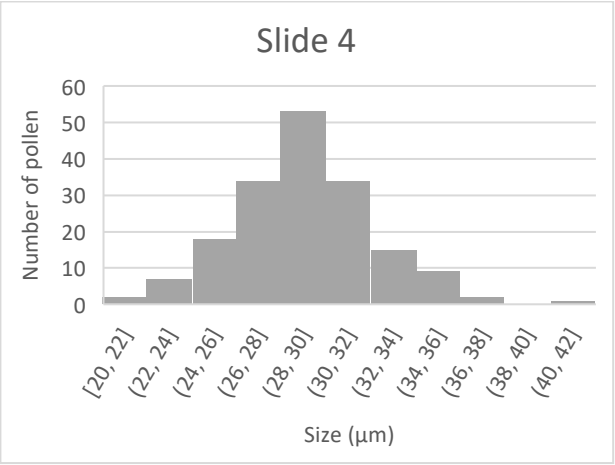
Appendix 1. Multiplicity

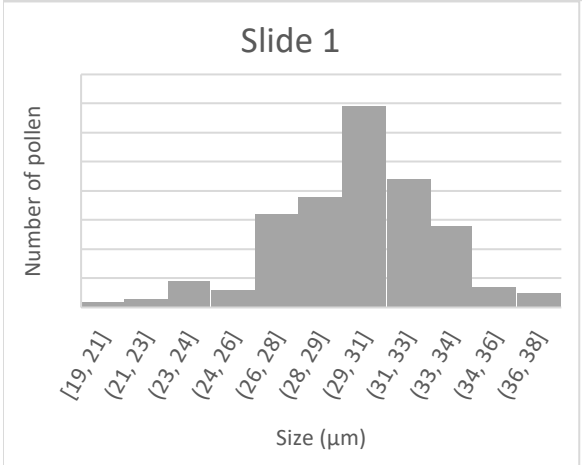
Slide	Height (m)	Traverses	Singles	Doubles	Triples	Tetrads	%
17	13.38	7	230	5	7	0	4.96
16	12.68	3	205	14	1	0	6.82
15	12.40	2	222	9	1	0	4.31
14	12.25	4	218	7	3	4	6.03
13B	11.82	9	235	1	0	0	0.42
13A	11.65	5	212	3	1	0	1.85
13	11.52	3	243	15	6	2	8.65
12	11.02	6	233	3	2	3	3.32
11	10.68	3	268	8	2	0	3.60
10	10.12	11	497	39	19	16	12.96
9	9.32	7	212	7	1	1	4.07
8	8.90	4	215	5	2	1	3.59
7	8.79	12	384	11	5	3	4.71
6	8.28	5	233	5	0	1	2.51
5	8.02	7	213	3	1	0	1.84
4	7.78	22	368	8	3	1	3.16
3	7.42	5	238	4	3	2	3.64
2	7.09	2	339	12	2	1	4.24
1	6.82	5	436	13	3	0	3.54
1A	6.81	5	664	34	20	12	9.04
0A	6.80	11	556	17	2	3	3.81
0	6.70	7	540	11	3	0	2.53
-1	6.52	3	282	4	2	0	2.08
-2	6.22	4	477	15	4	2	4.22
-3	6.05	5	470	15	9	3	5.43
-4	5.90	7	215	7	3	0	4.44
-5	4.45	7	221	0	0	0	0.00
-6	4.15	4	217	4	4	0	3.56
-7	3.46	7	525	21	2	2	4.55
-8	2.43	4	252	4	6	3	4.91
-9	1.38	4	222	4	3	0	3.06
-10	0.79	1	219	10	3	1	6.01
-11	0.69	14	629	21	6	3	4.55
-12	-0.12	2	213	4	2	0	2.74
-13	-0.41	4	228	3	2	0	2.15
-14	-1.01	4	243	2	1	0	1.22
-15	-1.51	3	423	5	1	2	1.86

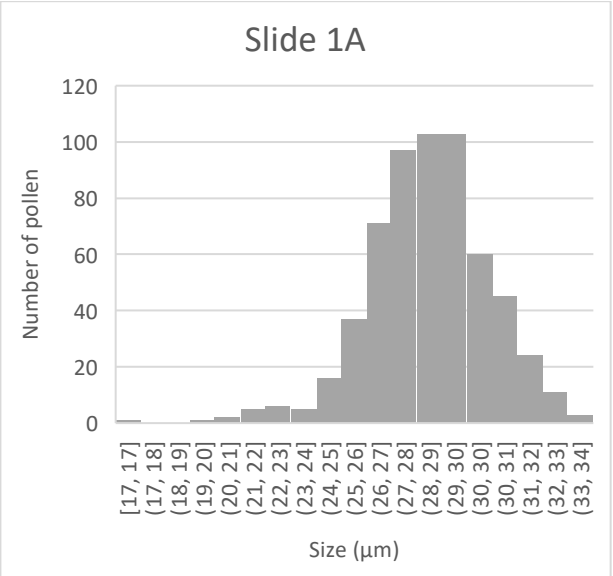
Appendix 2. Size histograms

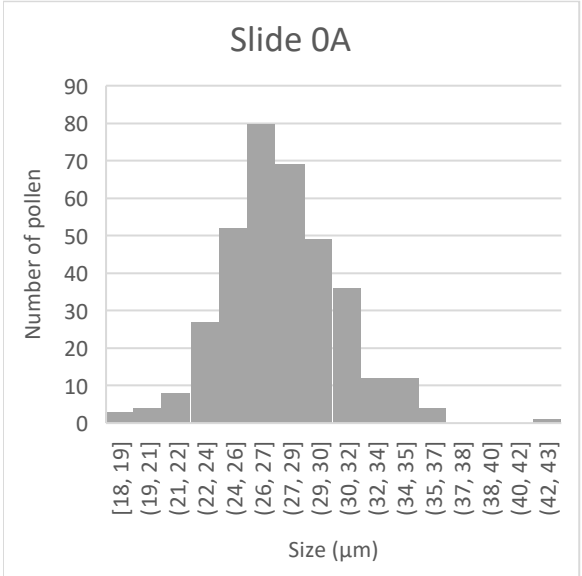


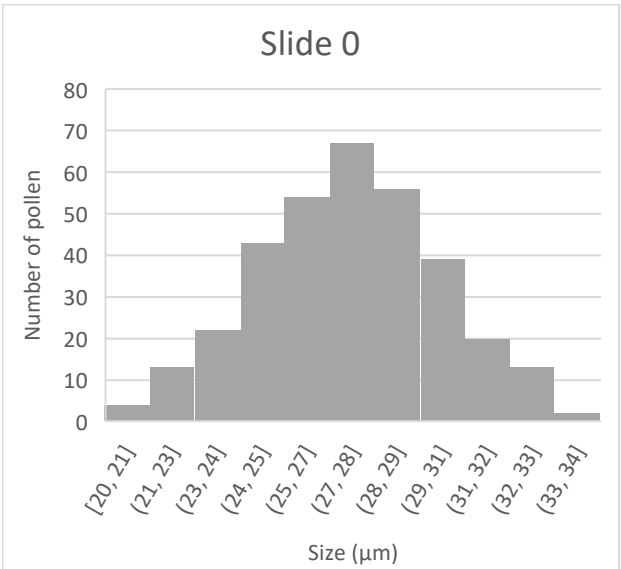


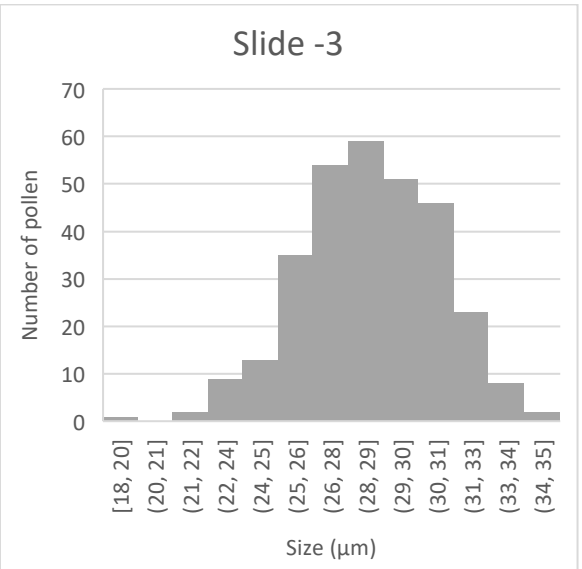


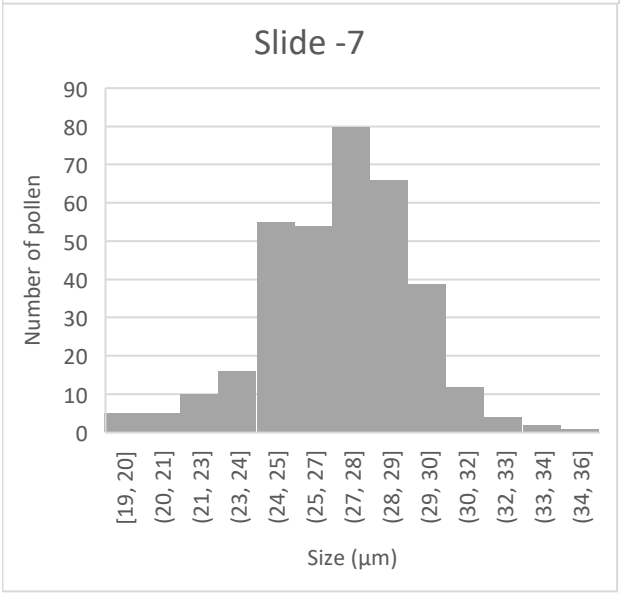


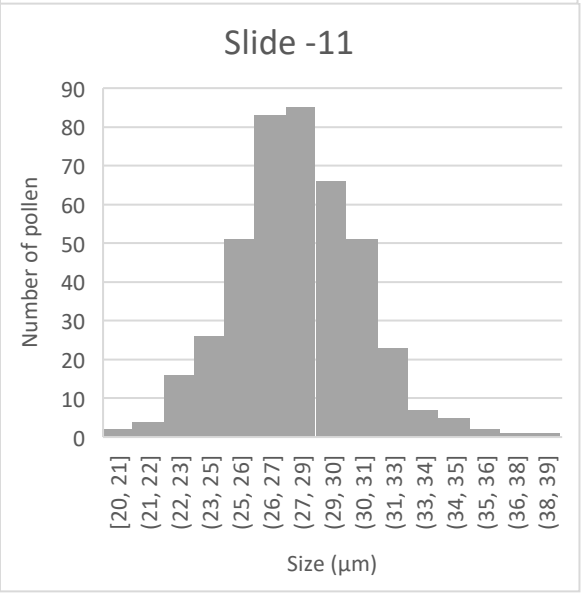





Slide 0
Number of pollen
Size (µm)
[20, 21]
(21, 23]
(23, 24]
(24, 25]
(25, 27]
(27, 28]
(28, 29]
(29, 31]
(31, 32]
(32, 33]
(33, 34]


Slide -3
Number of pollen
Size (µm)
[18, 20]
(20, 21]
(21, 22]
(22, 24]
(24, 25]
(25, 26]
(26, 28]
(28, 29]
(29, 30]
(30, 31]
(31, 33]
(33, 34]
(34, 35]


Slide -7
Number of pollen
Size (µm)
[19, 20]
(20, 21]
(21, 23]
(23, 24]
(24, 25]
(25, 27]
(27, 28]
(28, 29]
(29, 30]
(30, 32]
(32, 33]
(33, 34]
(34, 36]


Slide -11
Number of pollen
Size (µm)
[20, 21]
(21, 22]
(22, 23]
(23, 25]
(25, 26]
(26, 27]
(27, 29]
(29, 30]
(30, 31]
(31, 33]
(33, 34]
(34, 35]
(35, 36]
(36, 38]
(38, 39]

Appendix 3. Multiples found when measuring size

Slide	Absolute numbers							
	Doubles	Triples	Tetrads	Fives	Sixes	Eights	Tens	Total
10	22	10	8				1	399
7	4	3	1					196
4	3	1						175
1	7	1						243
1A	24	14	7	3	2	1	1	590
0A	8	2						357
0	3	1						333
-3	10	5	3					303
-7	16	1	1					349
-11	12	1	1					423

Slide	Percentages							
	Doubles	Triples	Tetrads	Fives	Sixes	Eights	Tens	Total
10	5.5	2.5	2.0				0.3	10.3
7	2.0	1.5	0.5					4.1
4	1.7	0.6						2.3
1	2.9	0.4						3.3
1A	4.1	2.4	1.2	0.5	0.3	0.2	0.2	8.8
0A	2.2	0.6						2.8
0	0.9	0.3						1.2
-3	3.3	1.7	1.0					5.9
-7	4.6	0.3	0.3					5.2
-11	2.8	0.2	0.2					3.3


UNIVERSITET
STOCKHOLMS
Stockholms
universitet